TRIBHUVAN UNIVERSITY

INSTITUTE OF ENGINEERING

PULCHOWK CAMPUS

THESIS NO : M-92-MSMDE-2023-2025

Modeling Electrochemical Corrosion in Magnesium Alloy Using Non-linear Phase Field Methods

by

Saroj Kumar Shah

A THESIS

SUBMITTED TO THE DEPARTMENT OF MECHANICAL AND AEROSPACE ENGINEERING IN PARTIAL FULFILLMENT OF THE REQUIREMENTS FOR THE DEGREE OF MASTER OF SCIENCE IN MECHANICAL SYSTEM DESIGN AND ENGINEERING

DEPARTMENT OF MECHANICAL AND AEROSPACE ENGINEERING

LALITPUR, NEPAL

April 17, 2025

COPYRIGHT

TRIBHUVAN UNIVERSITY

INSTITUTE OF ENGINEERING

PULCHOWK CAMPUS

DEPARTMENT OF MECHANICAL AND AEROSPACE ENGINEERING

The undersigned certify that they have read, and recommended to the Institute of Engineering for acceptance, a thesis entitled **"Modeling Electrochemical Corrosion in Magnesium Alloy Using Non-linear Phase Field Methods"** submitted by **Saroj Kumar Shah (079MSMDE019)** in partial fulfillment of the requirement for the degree of Master of Science in Mechanical Systems Design and Engineering.

Prof. Dr. Laxman Poudel

Supervisor,

Department of Mechanical and Aerospace Engineering

Er. Salim Maharjan

External Examiner,

Visiting Faculty,

Himalaya College of Engineering, Lalitpur

Tribhuvan University
Institute of Engineering
Department of Mechanical and Aerospace Engineering
Pulchowk Campus

Committee Chairperson,

Asst. Prof. Dr. Sudip Bhattrai

Head of Department,

Department of Mechanical and Aerospace Engineering

Date: April 7, 2025

ABSTRACT

Magnesium, recognized as the lightest structural metal with a density of approximately 1.7 g/cm^3, offers exceptional properties making it ideal for medical applications and lightweight engineering. Despite its advantages, such as environmental nontoxicity and ease of machining, its broader use is hindered by challenges such as poor corrosion resistance, necessitating ongoing research to enhance its structural and functional performance. This study presents an advanced phase field-based approach designed to predict the kinetics of pitting corrosion in magnesium alloy AZ31. The solid metal phase in the corrosion system is represented by an order parameter. The model integrates the electrochemical interactions at the electrolyte/metal interface, including the metal dissolution rate, electric potential distribution, and ionic concentration distribution. The evolution of ion concentration, order parameter, and potential distribution is guided by the minimization of the the total free energy of the system and is obtained by numerically solving the governing equations. The Multiphysics Object-Oriented Simulation Environment software (MOOSE Framework) is utilized for the implementation of numerical model. The model is validated with experimental results obtained from literature.

Keywords: *Phase field, Mg based alloys, Electro-chemical corrosion, Pitting corrosion, Electrolytes*

ACKNOWLEDGEMENT

The journey of completing this thesis has been one of perseverance, growth, and discovery, and it would not have been possible without the support and encouragement of many individuals.

First and foremost, I extend my deepest gratitude to my supervisors, Prof. Dr. Laxman Poudel, whose wisdom, patience, and unwavering support have guided me through every challenge. Their insightful feedback and encouragement have not only refined my research but also shaped my perspective on academic inquiry. I am truly fortunate to have had their mentorship.

I am also profoundly grateful to Department of Mechanical and Aerospace Engineering for providing the resources and a simulation research environment that enabled me to pursue this study. I also wish to acknowledge Er. Sachin Poudel for his generous support during simulation work. This thesis is not merely the result of individual effort but a reflection of the collective contributions of those who have supported, inspired, and believed in me. Furthermore, I am very grateful to the classmates of MSMDE batch 2079 for making academic journey, enriching & enjoyable.

CONTENTS

LIST OF FIGURES

LIST OF TABLES

LIST OF SYMBOLS

i^o = Exchange current

i_a = Anodic current α = Charge transfer coefficient

η = Overpotential

n = Charge on the ion

R = Universal gas constant

T = Temperature

F = Faraday's constant

J_{an} = Molar dissolution Flux

C_i = Molar concentration of species

R_i = Reaction term

D_i = Diffusion coefficient

z = Charge number

v = Fluid velocity

φ = Electrical potential

ϕ = Order parameter

LIST OF ABBREVIATIONS

Scanning Kelvin probe (SKP)

Scanning electrochemical microscopy (SECM)

X-ray diffraction (XRD)

Electron backscatter diffraction (EBSD)

Transmission electron microscopy (TEM)

Accelerated corrosion testing (ACT)

Relative humidity (RH)

Environmental scanning electron microscopy (ESEM)

Scanning electron microscopy (SEM)

Transmission electron microscopy (TEM)

X-ray photoelectron spectroscopy (XPS)

Auger electron spectroscopy (AES)

Secondary ion mass spectrometry (SIMS)

Fourier Transform Infrared (FTIR)

CHAPTER ONE: INTRODUCTION

1.1 Background

With a density of about 1.7 g / cm^3, magnesium is the lightest engineering metal. This is substantially less than that of titanium (Ti, 4.5 g/cm^3), iron (Fe, 7.9 g/cm^3), and aluminum (Al, 2.7 g/cm^3) (Kainer, 2003). In the twenty-first century, magnesium (Mg) is regarded as the best environmentally friendly substance (Xu et al., 2019). MIts primary chemical feature makes magnesium alloy a biodegradable material for use in medicine. Magnesium alloy's mechanical properties, such as its rigidity and plasticity, are specific to bioresorbable polymers (Hou et al., 2014). Magnesium alloys are known to have the highest strength-to-weight ratio of structural alloys, but their balance of properties, such as corrosion, ductility, and creep, is still being thoroughly studied. Other benefits of magnesium alloys include their remarkable damping capacity, their non-toxicity to the environment and human body (making them ideal for biodegradable implants), their ease of machining by high-speed milling and turning (they have a tool life that is 5–10 times longer than that of aluminum), and their versatility (they can be processed by rolling or extrusion) (Avedesian, 1999). However, a lot of obstacles still have to be removed before magnesium alloys can be used in more applications. Magnesium alloys' limited strength, poor plasticity, and poor corrosion resistance prevent them from being used in structural applications. In order to expand the use of magnesium alloys in the future, functional materials must address the issues of their rapid degradation rate (Song et al., 2020). However, engineers looking to reduce weight by using magnesium alloys still face difficulties due to corrosion (Gusieva et al., 2015). Traditional modeling approaches struggle to accurately capture the complex, non-linear nature of electrochemical corrosion in magnesium alloys, which is influenced by factors such as ion concentration, electric potential, and phase transformations (Jafarzadeh et al., 2019). While the phase field method has shown promise in simulating microstructural evolution, its application to electrochemical corrosion in magnesium alloys remains underexplored. The high susceptibility of magnesium alloys to electrochemical corrosion limits their industrial applications. Existing modeling methods fail to adequately describe the spatial and temporal evolution of corrosion. This research aims to develop a non-linear phase field model that accurately represents key variables and dynamics of the corrosion process, bridging the gap between experimental observations

and theoretical modeling to enhance predictive capabilities and improve magnesium alloy design.

When magnesium and its alloys are damp, a surface oxide or hydroxide layer forms quickly. This surface layer does not provide adequate corrosion protection since it is soluble in the majority of aqueous and humid environments, despite the large negative free energy of creation guaranteeing its quick formation (Taheri et al., 2012). A graphical representation that shows the stability of different phases of a metal (such as magnesium) as a function of electrode potential (E, in volts) and pH is called Pourbiax diagram (McCafferty and McCafferty, 2010). It helps predict whether a metal will corrode, remain passive, or be immune in a given environment. The Pourbaix (E - pH) diagram in figure 1.1 shows that Mg readily dissolves to form Mg^{2+} , with hydrogen evolution as the cathodic reaction across a wide pH range and is protected only in highly alkaline conditions where magnesium hydroxide becomes insoluble (Makar and Kruger, 1993).

Magnesium alloys are susceptible to galvanic and microgalvanic corrosion because of their very negative potential, even in deaerated environments, because oxygen is not needed for the primary cathodic water reduction reaction (Revie, 2008). The type of corrosion that occurs most frequently is pitting. Commercial magnesium alloys like AZ31 and AZ61 have already seen widespread reports of pitting corrosion (Martin et al., 2011). Pitting corrosion is still a major scientific difficulty despite a great deal of experimental investigation (Ernst and Newman, 2002). The dynamic changes in the electrochemical state at the electrolyte-metal contact and within the pit solution are the cause of this complexity. Additionally, the unpredictability of pit geometry and size limits make it difficult for experimental approaches to accurately determine the distribution of ionic species inside the pit solution. Using electrochemical kinetics and mass conservation, several computer models have been created to examine how the concentration of ions in pit solutions changes when metal dissolves (Sharland, 1987; Walton, 1990). These models explore electrochemical processes influenced by concentration gradients and electric fields. Since they don't take into consideration the dynamic evolution of the corrosion interface, they are frequently viewed as being oversimplified. Thanks to developments in numerical techniques, it is now possible to analyze the evolution of pit morphology using a variety of moving boundary models, including the peridynamics model, the finite volume approach,

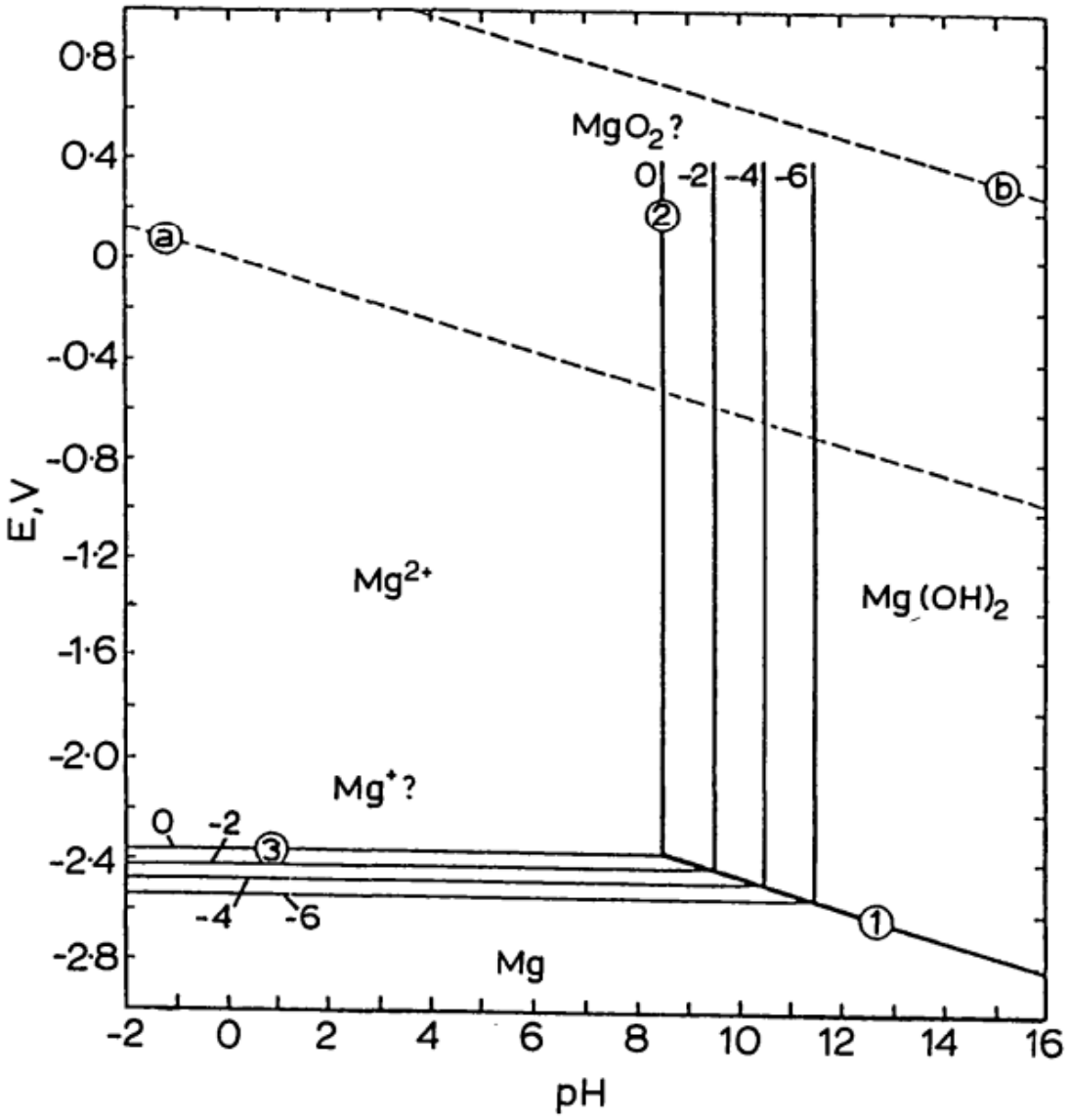

Figure 1.1: An illustration of phase equilibria for the magnesium-water system at 25°C using the Pourbaix (potential-pH) diagram (Makar and Kruger, 1993).

the arbitrary Lagrangian-Eulerian, the level set method, the finite element method, and the eXtended/Generalized FEM (Jafarzadeh et al., 2019). However, these methods face challenges like high computational costs, complex implementation, and difficulty handling intricate geometries. The phase field method has gained significant attention over the past three decades as an alternative approach for tracking moving interfaces. By introducing a continuous phase field variable, it effectively models complex microstructural evolution in processes like electrochemical corrosion.

1.2 Problem Statement

Magnesium alloys are widely valued for their excellent strength-to-weight ratio and biocompatibility, but their high susceptibility to electrochemical corrosion significantly limits their broader industrial applications. Despite numerous experimental studies, the complex and non-linear nature of the corrosion process, influenced by factors like ion concentration, electric potential, and phase transformations, remains inadequately captured by traditional modeling approaches. Existing methods often struggle to describe the spatial and temporal evolution of corrosion with sufficient accuracy, highlighting the need for advanced computational techniques. The phase field method, known for its ability to simulate microstructural evolution, presents a promising approach to address these limitations. However, its application to modeling electrochemical corrosion in magnesium alloys is still underexplored. This research aims to develop a non-linear phase field model that accurately captures the key variables and dynamics of the corrosion process, providing a comprehensive and predictive framework. By incorporating advanced numerical methods to enhance computational efficiency, this study seeks to bridge the gap between experimental observations and theoretical modeling, ultimately offering deeper insights into corrosion behavior and contributing to the improved design and longevity of magnesium alloys.

1.3 Research questions

How can phase field modeling effectively describe the electrochemical corrosion process in magnesium alloys?

This research seeks to explore the potential of phase field modeling as a robust and effective method for describing the complex electrochemical corrosion behavior observed in magnesium alloys. Magnesium alloys are widely used in industries like automotive, aerospace, and biomedical due to their low density, high strength-to-weight ratio, and biocompatibility. However, their high susceptibility to corrosion, particularly in aqueous environments, limits their broader applications. Understanding the electrochemical processes leading to corrosion is crucial for improving the longevity and reliability of these materials. Phase field modeling, a powerful computational technique, offers a way to simulate the microstructural evolution of materials over time by solving non-linear differential equations based on thermodynamic and kinetic principles. This study aims to investigate how well phase field methods capture the key variables of the corrosion process, such as ion concentration, electric potential, and the phase evolution of the alloy material. Through this investigation, the research intends to evaluate the strengths and limitations of phase field modeling in corrosion analysis and determine whether this approach can offer insights beyond conventional modeling techniques. The ultimate goal is to enhance the predictive capability and computational efficiency of corrosion models for magnesium alloys, providing a strong foundation for future experimental validation and industrial application.

1.4 Significance/Rationale of the study

This research is essential due to the widespread use of magnesium alloys in automotive, aerospace, and biomedical industries, where their lightweight and high-strength properties are often limited by their high susceptibility to electrochemical corrosion. By developing a non-linear phase field model, this study aims to provide a more accurate and predictive framework for understanding corrosion behavior, addressing gaps left by traditional modeling methods. The outcomes will benefit material scientists, engineers, and manufacturers by offering better tools to design corrosion-resistant materials, reduce maintenance costs, and improve the safety and longevity of magnesium-based components. This research also supports advancements in biodegradable medical implants by ensuring controlled degradation and bio-compatibility.

1.5 Objective

1.5.1 Main Objective

- The major objective is to create a numerical model for electrochemical corrosion in Magnesium alloy by using Phase Field method and study the corrosion behaviour.

1.5.2 Specific Objectives

- To study kinetics of ion migration in corrosion system.
- To develop two phase system with focusing the study to single composition.
- To obtain material properties, initial conditions and boundary conditions specifically for AZ31 Mg Alloy from literatures.
- To solve for the phase field variables, composition variables and electric potential.
- Analyse the result of simulation.

CHAPTER TWO: LITERATURE REVIEW

2.1 Electrochemical Corrosion

Metal valence electrons are transferred to electrochemically active ions and molecules in the metal's surroundings, and a chemical reaction transforms the chemical state of metal atoms into metal ions, forming metal corrosion. Thus, the term electrochemical corrosion is used to describe metal corrosion. Whether a metal will corrode in a certain environment is determined by thermodynamics. The metal's rate of corrosion in a particular environment is determined by kinetics (Tait, 2018).

2.1.1 Corrosion Thermodynamics

Electrochemical processes can be separated into a minimum of two half-reactions, wherein chemical species either receive or lose electrons. This oxidation, known as the anodic half-reaction, takes place at areas on the metal surface called anodes. Regions known as cathodes are where the cathodic half-reaction, which reduces electrochemically active species in the electrolyte, takes place. These anodes and cathodes may be microscopic or visible to the naked eye and can be separated by measurable distances. To preserve electrical charge neutrality, negative and positive ions in the electrolyte move toward the anodes and cathodes, respectively (Buchanan and Stansbury, 2005). For example, consider the following corrosion reaction of Iron immersed into Hydrochloric acid:

$\mathrm{Fe} + 2\,\mathrm{HCl} \longrightarrow \mathrm{FeCl_2} + 2\,\mathrm{H_2}$

The above reacction is the sum of the following half reactions:

$\mathrm{Fe} \longrightarrow \mathrm{Fe^{2+}} + 2\,\mathrm{e^-}$ Anodic half-reaction

$2\,\mathrm{H^+} + 2\,\mathrm{e^-} \longrightarrow \mathrm{H_2}$ Cathodic half-reaction

A corrosion reaction, such as the iron half-reaction, can occur in both forward and reverse directions, involving both oxidation and reduction processes. Equilibrium is reached when the rates of these forward and reverse reactions become equal. While other atoms exit the surface and change into ions, metal ions stay close to the metal surface at this point, establishing a dynamic balance that allows metal ions to potentially return to the lattice of metal and return to metal atoms. The resultant thin equilibrium layer is made up of positively charged metallic ions near the surface, water molecules deposited on the metal surface, and the negatively charged states of the valence electrons of the surface

atoms. As seen in figure 2.1, this layer is known as the electrical double layer (EDL) (Tait, 2018).

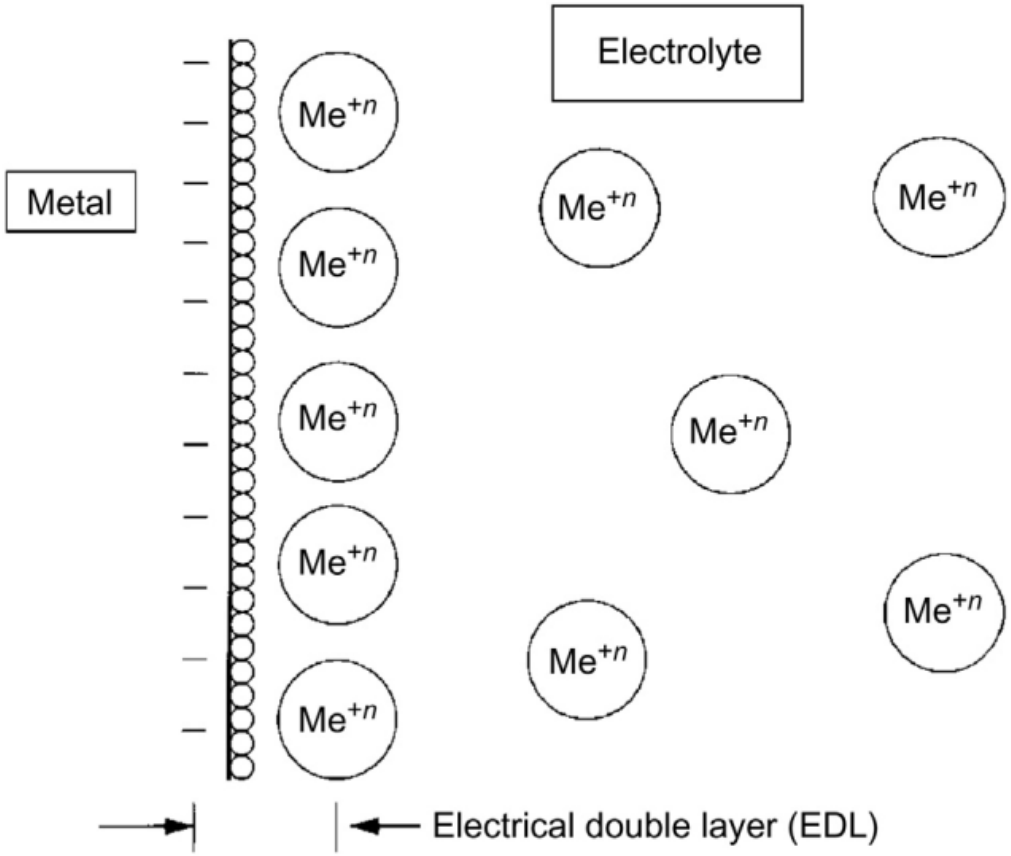

Figure 2.1: An Electrical Double Layer Equilibrium Model

The charge separation within an EDL generates an electrical potential, which can be measured as the voltage difference between two metal and a reference electrode(e.g., a hydrogen reference electrode), using an external connection to an electrometer as shown in figure 2.2 (Keithley Instruments, 1984). When the electrode potential is measured without any applied external potential, it is referred to as the open circuit potential (OCP) or corrosion potential. By measuring the OCP of a test electrode, it is possible to predict whether corrosion is likely to occur in a specific metal-environment combination.

The OCP is linked to Gibbs free energy through the equation 2.1 , which shows whether corrosion will happen. If the Gibbs free energy ΔG is negative, the metal will corrode.

$$\Delta G = -nFE \tag{2.1}$$

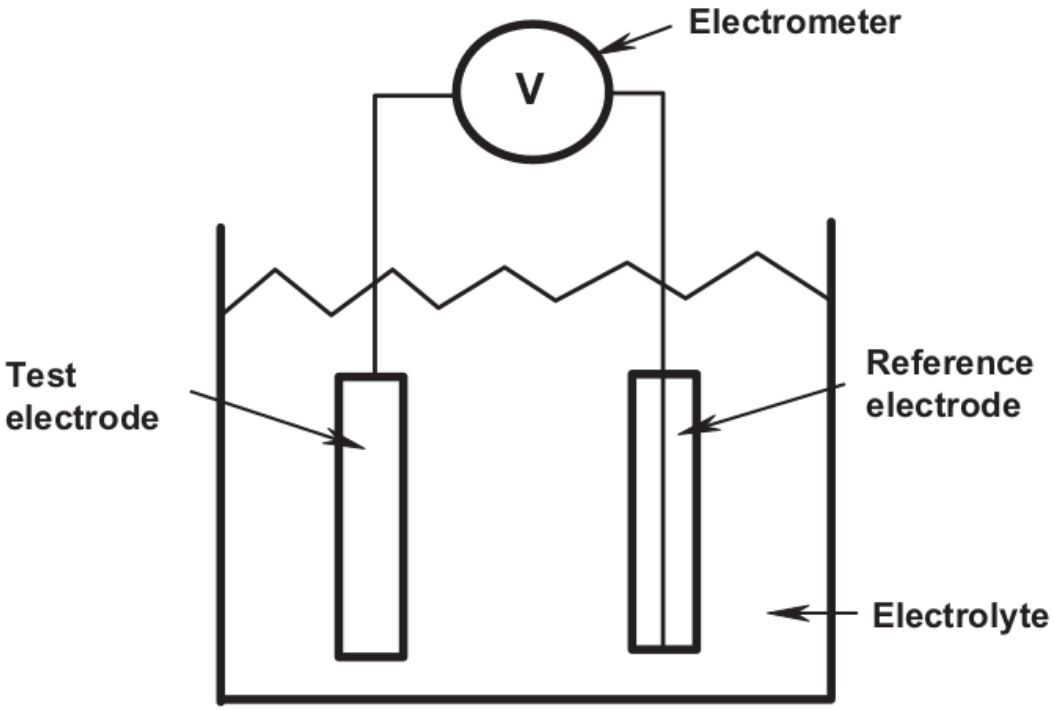

Figure 2.2: Schematic for measuring electrode potential (differences).

where ΔG is the Gibbs free energy, n is the number of electrons in the anodic corrosion reaction, F is Faraday's constant in 96,500 C, E is the OCP (corrosion). Because OCP magnitudes fluctuate in response to changes in EDL composition, they are not inherent characteristics of a metal. An EDL's composition will also alter in response to an applied voltage. EDL composition is mathematically related to OCP by the Nernst equation 2.2 (Vetter, 2013).

$$E = E^o - (RT/nF)ln(a_{products}/a_{reactants}) \tag{2.2}$$

where a is the chemical activity of products and reactants, E is the measured potential in volts or millivolts. E^o is the OCP when all activities in Eq. 2.2 are equal to 1, R is the ideal gas constant which is equal to 1.986 cal/mole K, T is the temperature in degrees Kelvin (K), n is the number of electrons in the anodic half reaction, F is Faraday's constant, which is equal to 96,500 C. The quantity RT/F is equal to 25.6 mV-equivalents at 298K (25C).

2.1.2 Corrosion Kinetics

When the OCP is positive, spontaneous corrosion is anticipated. However, when spontaneous corrosion is anticipated by Eq. 2.2, the metal OCP for specific conditions

does not tell us how quickly the corrosion will progress. Estimating corrosion rates and comprehending the movement of electrons from the metal to electrochemically active ions in the environment are made possible by corrosion kinetics.

There will be a difference between the electrode's OCP and the equilibrium potentials of the half-reactions occurring on its surface. Charge transfer overvoltage, also known as activation overvoltage, is the difference between the actual potential and the equilibrium potential for a certain reaction where the reactant and product concentrations at the electrode surface match those in the bulk solution η. This discrepancy results from the non-instantaneous rate of charge transfer at the electrode-electrolyte contact. It's crucial to remember that when mass transport is substantially quicker than charge transfer, the concentration at the electrode surface corresponds to the bulk concentration. The Butler-Volmer equation describes the relationship between the driving force (potential E) and the reaction rate (expressed by current density i) for reactions when the rate is constrained by activation overvoltage (Frankel, 2016).

$$i = i_0 Exp[\frac{\alpha n F \eta}{RT}] - i_0 Exp[\frac{-(1-\alpha) n F \eta}{RT}] \tag{2.3}$$

where n is the ion's charge in equivalents/mol, F is the Faraday constant = 96,487 C/equivalent, R is the gas constant = 8.314 J/mol-K, and α is the unitless charge transfer coefficient. Since α is usually about 0.5, it must be between 0 and 1. At high overpotentials, the Butler-Volmer equation becomes easier to:

$$i_{net} = i_0 Exp[\frac{\alpha n F \eta}{RT}] \tag{2.4}$$

2.1.3 Pitting Corrosion

Pitting is one of the most destructive forms of corrosion because it occurs in small, localized areas that are difficult to detect, yet it has a significant impact on structural integrity (Yu et al., 2016, Akpanyung and Loto, 2019). pitting corrosion mechanism can be divided into two stages as pit initiation and pit growth stage.

Pit Initiation: Pit initiation can happen on the weak spot like compositional inhomogenity, local stress section, local scratch, local change in chloride concentration, microstructural pattarn on the metal surface.

Pit Growth: In this stage, consider a small pit has already been formed on the metal surface as shown in figure. At the pit, depletion of oxygen occurs while at the surface other than pit, depletion of oxygen occurs. This imbalance in oxygen concentration makes the pit to work as anode surface where oxidation of metal to metal ions occurs and the other surface work as cathode where reduction of oxygen takes place. The oxidized metal ions react with hydroxide ions to form metal-hydroxide (corrosion product). After sometime when the corrosion product reaches its solubility but the dissolution of metals still occurring since the demand for electrons near cathodic site is high as cathode region is large. The excess metal ions (accumulated +ve charge) attract chlorine ions (-ve charge) from the bulk electrolyte (NaCl solution) to maintain charge neutrality. The metal ions combine with chlorine ions to form metalchloride which then reacts with water molecules to form metal hydroxide and hydrochloric acid (hydrolysis reaction). The hydrogen ion of acid reduces the pH near the pit and supports pit growth according to purbiax diagram and also the presence of chlorine ion disturbs the re-passivation process. The kinetic growth of pit is dependent on the electrolytic diffusion rate within the pit (Akpanyung and Loto, 2019).

2.1.4 Corrosion Analysis method

Corrosion analysis methods for magnesium alloys encompass a variety of techniques aimed at understanding and mitigating corrosion processes. Key electrochemical techniques, such as electrochemical impedance spectroscopy, provide crucial insights into corrosion rates and mechanisms by measuring the electrochemical behavior of Mg alloys in different environments. Localized electrochemical techniques, including scanning Kelvin probe (SKP) and scanning electrochemical microscopy (SECM), offer high spatial resolution to identify and map localized corrosion activities, revealing areas susceptible to corrosion initiation and propagation. Non-electrochemical methods, such as X-ray diffraction (XRD), electron backscatter diffraction (EBSD), and transmission electron microscopy (TEM), are employed to characterize the microstructure and composition of corrosion products, providing detailed information on the phases and compounds formed during corrosion. Additionally, field exposures and accelerated corrosion testing (ACT) are utilized to simulate real-world conditions, enabling the evaluation of Mg alloys' durability and performance in various environments. Laboratory exposures at constant relative

humidity (RH) and environmental scanning electron microscopy (ESEM) further enhance the understanding of corrosion behavior under controlled conditions. Collectively, these methods offer a comprehensive and multifaceted approach to studying and improving the corrosion resistance of magnesium alloys, facilitating the development of more durable and reliable materials for various applications. Analytical methods utilizing advanced microscopy techniques such as scanning electron microscopy (SEM) and transmission electron microscopy (TEM), which provide high-resolution images of corrosion morphology and microstructural changes are also being used in corrosion analysis. Spectroscopic techniques like X-ray photoelectron spectroscopy (XPS) and Auger electron spectroscopy (AES) are used to analyze the elemental composition and chemical states of corrosion products on the alloy surface. Secondary ion mass spectrometry (SIMS) allows for the detection and mapping of trace elements and impurities that influence corrosion behavior. Additionally, Fourier Transform Infrared (FTIR) spectroscopy and Raman spectroscopy offer molecular-level insights into the corrosion products and interactions between the alloy and its environment. These analytical tools, combined with statistical analysis and three-dimensional imaging techniques, create a comprehensive framework for investigating and mitigating corrosion in magnesium alloys, driving advancements in material performance and reliability (Esmaily et al., 2017).

2.2 Magnesium and its alloy

Magnesium and its alloys are renowned for being the lightest structural metallic materials, making them highly valuable in industries where weight reduction is critical, such as automotive, aerospace, and electronics. The low density of magnesium alloys translates to improved fuel efficiency and reduced emissions in transportation applications, significantly impacting environmental sustainability. Additionally, their high strength-to-weight ratio makes them ideal for components that require both lightness and durability, such as aircraft parts, automotive components, and portable electronic devices. Magnesium alloys also exhibit good electromagnetic shielding properties, making them suitable for electronic housings and mobile devices, enhancing both performance and durability in these applications. Moreover, their ability to absorb energy makes them valuable in crash-resistant structures, contributing to safety advancements in automotive and aerospace engineering.

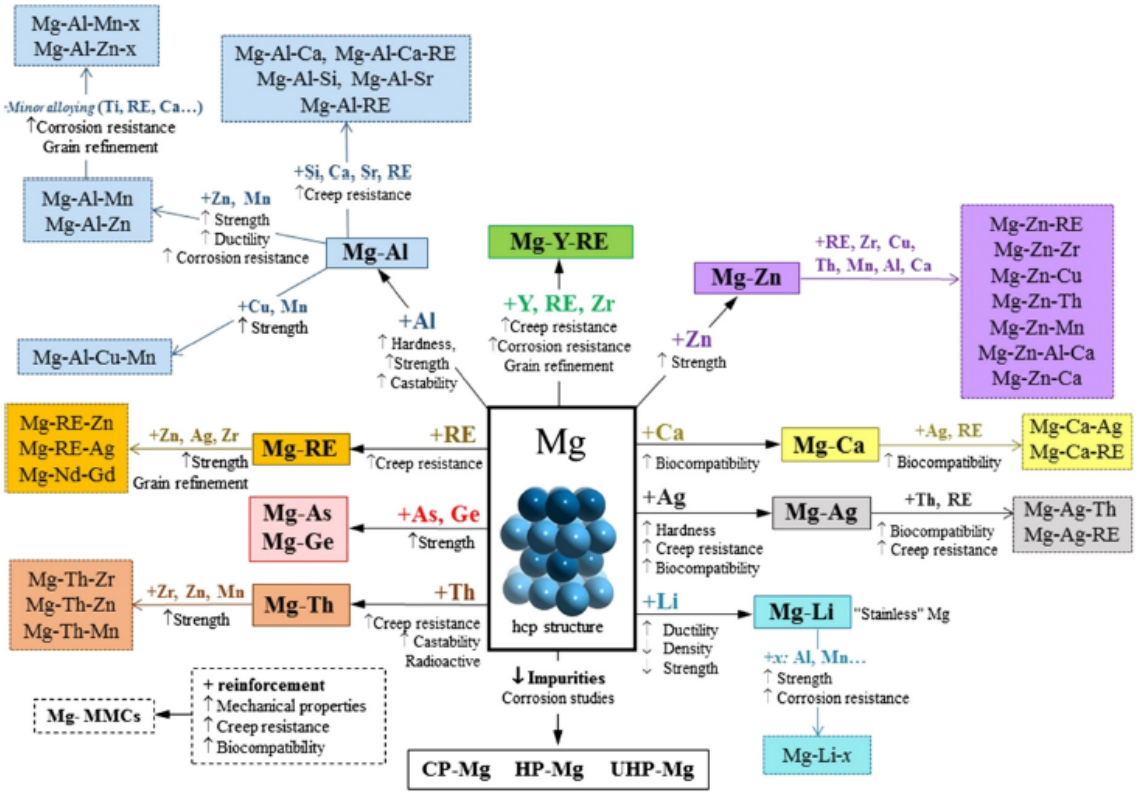

Figure 2.3: Magnesium Alloy

Despite these advantages, magnesium's high reactivity and susceptibility to corrosion present significant challenges. Magnesium alloys corrode more readily than other structural metals, which can compromise their structural integrity and performance over time. Therefore, understanding and improving the corrosion resistance of magnesium alloys is crucial for their broader application. Effective corrosion analysis helps in developing protective coatings, alloying strategies, and treatment processes to enhance the longevity and reliability of magnesium components. These advancements are essential not only for extending the service life of magnesium-based products but also for ensuring safety and performance in critical applications. By addressing these corrosion challenges, researchers and engineers can drive innovation and facilitate the wider adoption of magnesium alloys, capitalizing on their unique properties to meet the demands of modern technology and sustainability goals (Esmaily et al., 2017). The selection of AZ31 magnesium alloy for this thesis is justified by its exceptional combination of mechanical properties, lightweight nature, and corrosion resistance, making it a highly attractive material for various engineering applications. AZ31 is a widely used magnesium alloy due to its excellent strength-to-weight ratio, which is particularly beneficial in the automotive and aerospace

industries for reducing overall weight and enhancing fuel efficiency. Additionally, the alloy's good formability and weldability facilitate its use in complex component manufacturing. AZ31 also exhibits favorable electrochemical properties, making it a suitable candidate for studies on corrosion behavior and ion migration. By focusing on this alloy, the research aims to address practical challenges in material performance and contribute to the development of more durable and efficient magnesium-based components.

2.3 Phase Field Method

As opposed to sharp interface models, which require tracking the evolution of specific interfaces, the phase field method has proven to be incredibly effective at visualizing the development of microstructure. The approach also makes it possible to treat numerous physical events at once within the context of irreversible thermodynamics.

The order parameter ϕ is the only variable that continually represents the state of the entire microstructure in the phase field technique. For instance, the precipitate is represented by $\phi = 1$, the matrix by $\phi = 0$, and the interface by $0 < \phi > 1$. Thus, the latter can be identified by the area where w shifts from its precipitate value to its matrix value. The interface's width is the range over which it varies. The phase field is the collection of order parameter values across the entire volume. After that, the order parameter and its gradients are used to characterize the volume's total free energy F. The pace at which the structure changes over time is determined using irreversible thermodynamics and is dependent on how F changes with ϕ. The evolution of structure is driven by gradients in thermodynamic variables.

2.4 Related work

A specific kind of localized corrosion known as pitting corrosion occurs when the rate of corrosion is higher in some places than in others. Many alloys, such as magnesium alloy, which are shielded from general corrosion by a passive coating on their surface, exhibit pitting corrosion damage (Frankel, 1998; Jones, 1996; Marcus and Oudar, 2002). This electrochemical equilibrium diagram for the Mg-H_2O system shows that while magnesium and its alloys corrode in neutral and acidic solutions, they passivate in strong alkaline conditions (Pourbaix, 1966). Recent reports have revealed an intriguing phenomenon

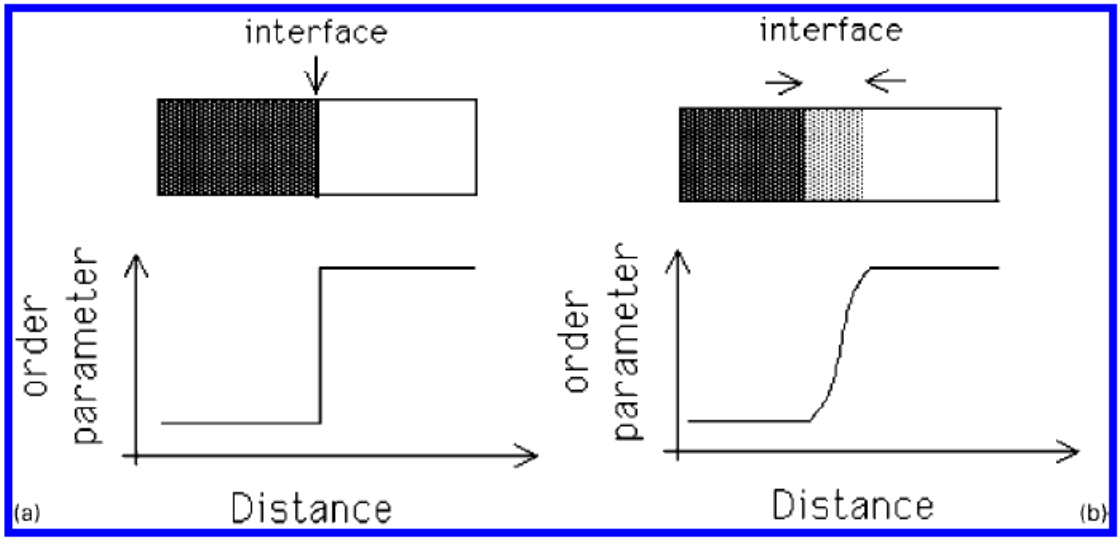

Figure 2.4: (a) Sharp Interface (b) Diffuse Interface

related to the passivation of magnesium and its alloys in very alkaline solutions: the oxide layers had sporadic ruptures that resulted in pitting under open circuit conditions (Taheri and Kish, 2012; S. Li et al., 2016). When solid metal corrodes, the usual processes include the material dissolving due to electrochemical interactions with an electrolyte at the metal surface, the dissolved metal ions being transported in the electrolyte, and the corrosion-induced mechanical degradation of the material (Jafarzadeh et al., 2019). Pitting corrosion is the localized corrosion which is the most destructive type of corrosion. The anodic reaction at the pit surface, which causes metal dissolution, is the main cause of pitting corrosion in metals exposed to aqueous solutions. The pitting corrosion process in magnesium alloy can be illustrated by the figure 2.5, where we can see the metal surface in the pit is directly exposed to the electrolyte makes it anode and the surface covered by passive film work as cathode. The metal ions get dissociated from metal surface at anode and release electron which then travels to cathode surface where reduction reaction takes place and electrons gets consumed. Pit growth models are based on the transport kinetics of species within the electrolyte and the dissolution kinetics at the corrosion front.

The general form of this anodic reaction is given by:

$\mathrm{M(s)} \longrightarrow \mathrm{M^{z+}(aq)} + \mathrm{ze^-}$ anodic reaction

Where e^- indicates an electron, $M^{z+}(aq)$ is the dissolved metal ion with charge number z in the aqueous solution, and $M(s)$ is a generic metal atom in the solid state. When an electrolyte is present, the anodic reaction causes localized metal dissolution, as seen

in figure 2.5. The anodic reaction produces electrons that go through the solid metal and take part in cathodic reactions, which usually take place outside the pit. The cathodic processes produce precipitated solid particles and corrosion products such hydrogen gas (H_2).

$2\,H_2O\,(aq) + 2\,e^- \longrightarrow H_2(g) + 2\,OH^-(aq)$ reaction at cathode

$Mg^{2+}(aq) + 2\,OH^-(aq) \longrightarrow Mg(OH)_2(s)$ formation of product

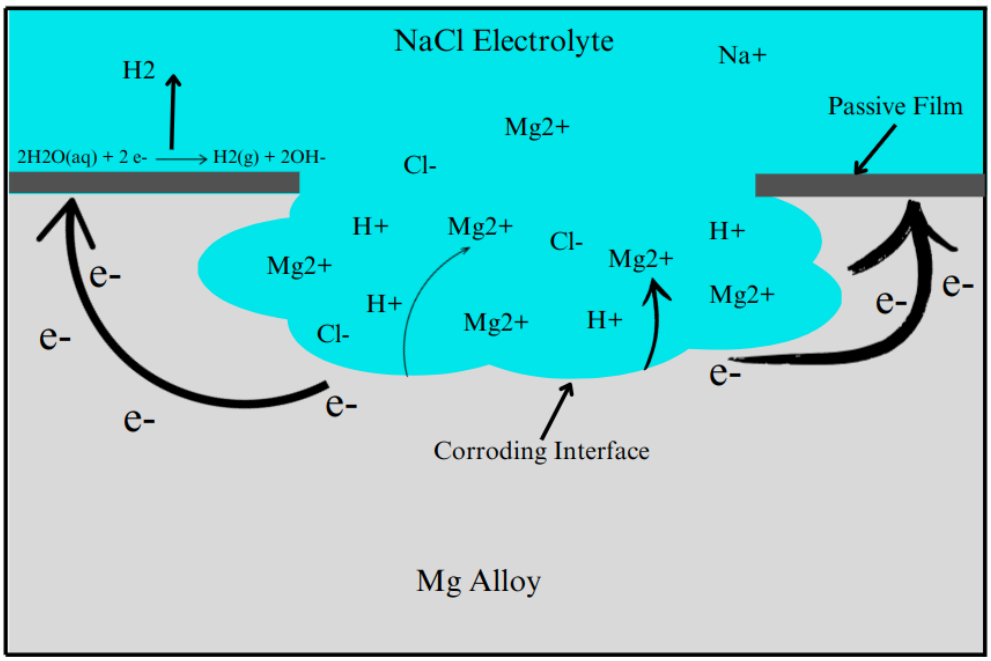

Figure 2.5: Schematic of metal dissolution by the anodic reaction.

The anodic reaction rate can be expressed in tafel approximation of Butller-Volmer equation as (Jafarzadeh et al., 2019; Frankel, 2016):

$$i_a = i_0 \exp\left(\frac{\alpha F \eta}{RT}\right) \tag{2.5}$$

The anodic current density is denoted by i_a, the exchange current density by i_0, the overpotential by η, Faraday's constant by F, the gas constant by R, the absolute temperature by T, the transfer coefficient by α, and another by i_a.

Given the molar dissolution flux (J_{an}) at the corrosion front, the anodic current density (i_a) scales linearly with it (Jafarzadeh et al., 2019; Tait, 2018):

$$i_a = nF|J_{an}| \tag{2.6}$$

The transport of ionic species in the electrolyte is influenced by diffusion and migration effects. The general equation for species transport in solution is (Jafarzadeh et al., 2019):

$$\frac{\partial C_i}{\partial t} = -\nabla \cdot J_i + R_i \tag{2.7}$$

where C_i is the molar concentration of species i, J_i is the molar flux, and R_i is the reaction term. The transport flux of charged species is governed by (Jafarzadeh et al., 2019):

$$J_i = -\left[D_i \nabla C_i + z_i \frac{D_i F}{RT} C_i \nabla \varphi - v C_i\right] \tag{2.8}$$

where D_i is the diffusion coefficient, z_i is the charge number, φ is the electric potential, and v is the fluid velocity.

The evolution of interfaces between phases in a variety of physical phenomena, such as solidification, microstructural evolution, and phase transitions in ferroelectric and ferromagnetic materials, has been widely simulated using Phase-Field (PF) modeling, also referred to as diffuse interface modeling. PF models have recently been modified to model corrosion with an emphasis on the metal-electrolyte interface's evolution.

A lot of work has gone into creating numerical models for pitting corrosion in the last few decades. The two difficult issues that the majority of these numerical models encounter are the shifting interface and the electrical double layer at the metal/electrolyte interface. The corroding surface has typically been represented by a sharp interface in these modeling attempts, necessitating a matching mesh at each time step (Sarkar et al., 2012; Xiao and Chaudhuri, 2011). Errors and calculation costs associated with violations of mass conservation laws are increased as a result. Over the last three decades, the phase field (PF) method has become a potent simulation tool for simulating the evolution of microstructures. Applications of the PF approach are numerous and include solidification, dendritic growth, solute diffusion and segregation, phase transformation, electrochemical deposition, dislocation dynamics, crack propagation, void formation and migration, gas bubble evolution, and electrochemical processes (Y. Li et al., 2017).

Because PF models presume a diffusive boundary at the phase boundaries instead of a sharp one, the mathematical functions at the interface are continuous. On a finite thickness diffuse contact, the phase field variable $\phi(x,t)$ that fluctuates between 0 and 1 is used in the PF corrosion model (Mai et al., 2016; Ansari et al., 2018). This model couples two partial differential equations (PDEs): the Allen-Cahn equation, which governs phase transitions, and the Cahn-Hilliard equation, which describes the evolution of metal-ion concentration.

$$\frac{\partial \phi}{\partial t} = -L\frac{\delta \mathcal{F}}{\delta \phi} \tag{2.9}$$

$$\frac{\partial C}{\partial t} = \nabla \cdot \left(M \nabla \frac{\delta \mathcal{F}}{\delta C} \right) \tag{2.10}$$

The system minimizes the total free energy functional $\mathcal{F}(\phi, C)$, where parameters like L (controlling corrosion rate) are adjusted to reflect different corrosion behaviors, such as activation-controlled corrosion. PF corrosion models have been used to simulate pitting, galvanic, and stress-dependent corrosion, primarily in 2D, with recent advancements into 3D simulations. Several studies have extended the phase field method to simulate corrosion phenomena in different environments. Initially, it was formulated for corrosion in a dual-oxidant system (Abubakar et al., 2015). Based on this, Mai et al. (Mai et al., 2016) created a phase field model for pitting corrosion that was based on the Kim–Kim–Suzuki (KKS) model. The Tafel relation was used to connect the interface kinetics parameter to the corrosion current density. Nevertheless, the electrolyte domain was not included in their model. This was later enhanced by Tsuyuki et al. (Tsuyuki et al., 2018), who developed a qualitative overview of corrosion behavior by connecting the interface kinetics parameter to pH. Nevertheless, the predictions of their model did not match the experimental facts. Later, in order to examine the function of insoluble products of corrosion in pitting corrosion, Ansari et al. put forth a different phase field model that concentrated on reaction kinetics.

By including solids' mechanical behavior in the interface kinetics parameter or total free energy, phase field modeling has advanced to handle stress corrosion cracking and mechanically assisted corrosion. While some models have included the electrolyte domain, many fail to account for ion diffusion and migration, resulting in incomplete electrochemical descriptions. Cui et al.Cui et al., 2023 highlighted the importance of considering electrolyte domain size in KKS-based models, showing that ion transport

limitations significantly affect corrosion predictions.

In this study, a PF method is used to model uniform corrosion considering the anodic reaction of the Magnesium alloy AZ31, the transport of metal ions and the distribution of electric potential in the electrolyte.

CHAPTER THREE: METHODOLOGY

3.1 Conceptual Framework

3.1.1 Literature Review

A literature review is a piece of academic writing demonstrating knowledge and understanding of the academic literature on a specific topic placed in the context. It is the first phase in the research methodology. It will be conducted with the help of different books, academic reports from campus library and scholarly articles. The study will then be directed towards the phase field modeling technique and its application for corrosion analysis. In context with the electrochemical corrosion in Magnesium alloy, different academic writings including journal papers, reports, books, etc. will be referred. This will provide the necessary foundation to carry out the thesis effectively. With the review of some studies in this field, a research gap is identified to formulate a problem statement and further literatures will be reviewed along the course of this research work in order to fill the research gap.

3.1.2 Formulating of Phase Field Model

With the understanding of fundamental concepts of phase field method and the associated physics of electrochemical corrosion in Mg alloy the mathematical models will be developed that describe the corrosion process. This involves creating the phase field equations, which include variables such as the concentration of ions, the electric potential, and the order parameter that represents the phase of the material. These equations are based on fundamental electrochemical principles and phase field theory.

3.1.3 Initialize Phase Field Parameters

The initial conditions for the simulation, including the material properties of the Mg alloy, geometry of the domain (square geometry of 400 micrometers), the initial distribution of ions, the initial phase field configuration, and environmental conditions such as temperature and electrolyte concentration shall be determined. These parameters are critical for accurately simulating the corrosion process.

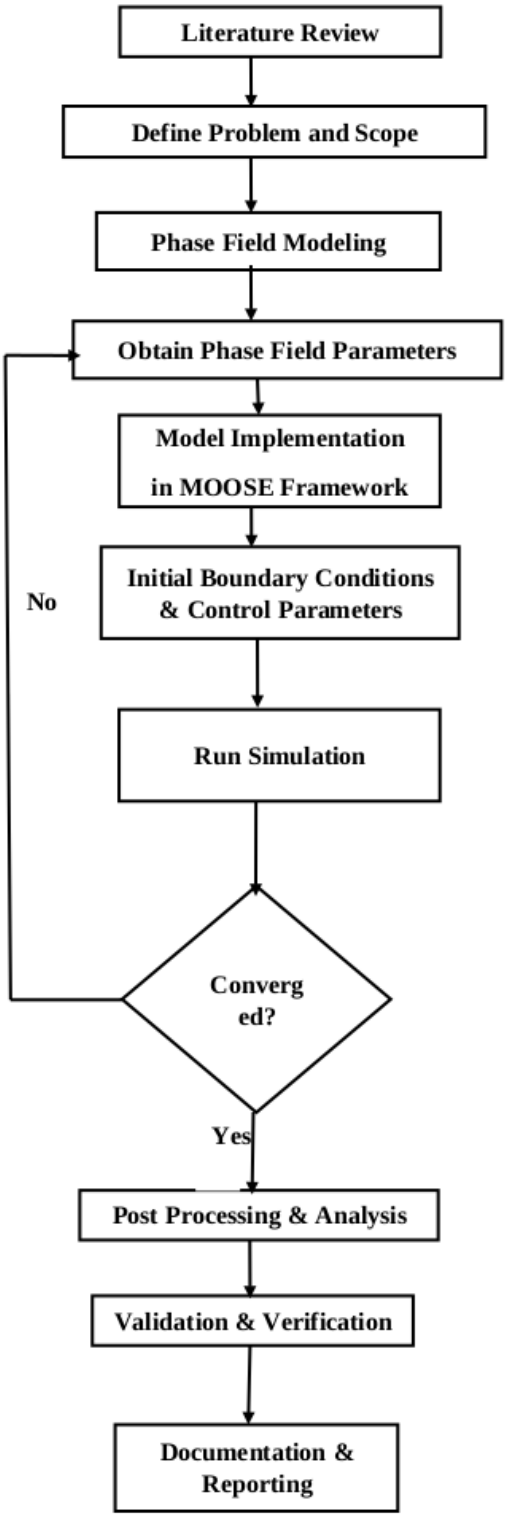

Figure 3.1: Work Flow Chart.

3.1.4 Solving for significant variables

Numerical methods shall be used to solve the formulated phase field equations over the specified time period. A software named MOOSE (Multiphysics Object Oriented Simulation Environment) framework shall be used for solving the differential equation The software is an open-source, parallel finite element method (FEM) framework utilized for complex simulations. For solving the nonlinear equations involved in the simulation, the Preconditioned Jacobian-Free Newton-Krylov (JFNK) method shall be implemented, which efficiently handles the computational challenges associated with nonlinear systems. To enhance computational efficiency and enable parallel processing, the Additive Schwartz Method (ASM) is applied for domain decomposition. This approach divides the simulation domain into smaller subdomains, allowing for more efficient and scalable problem-solving. The geometry of the domain, while not impacting the underlying physics of the simulation, is standardized to a square domain with dimensions ranging from 200 to 600 micrometers, providing a consistent reference for the simulations.

3.1.5 Finding and Report Submitting

The findings of the research study will be systematically documented and submitted to the department as the thesis report according to the requirement of the Department of Mechanical Engineering.

3.2 Phase field formulation

3.2.1 General Consideration

Figure 3.2 schematically illustrates a corrosion system consisting of AZ31 magnesium alloy as a metallic solid phase submerged in NaCl solution. Even while a passive coating that protects the metal surface from general corrosion can fail locally, the metallic surface may get exposed to the corrosive environment, which would start the dissolution process and release cations into the electrolyte. While it is feasible to simulate pit initiation by adding a random term to the phase field formulation (Kovacevic et al., 2023), in this work we concentrate on the propagation of an existing pit by taking into account anodic and cathodic reactions, ionic species transport, and the dependence of the overpotential on the concentration of metal ions in the electrolyte. It is anticipated that in this system, no new

passive film will form. The following discusses electrochemical reactions.

For the oxidation of main metal alloy in AZ31.

$Mg \longrightarrow Mg^{2+} + 2\,e^-$

$Al \longrightarrow Al^{3+} + 3\,e^-$

$Zn \longrightarrow Zn^{2+} + 2\,e^-$

The above reaction can be simplified to the following anodic reaction.

$M \longrightarrow M^{n+} + ne^-$

Similarly,

$Mg^{2+} + H_2O \longrightarrow Mg(OH)_2 + H^+$ (primary hydrolysis)

$H_2O \longrightarrow OH^- + H^+$ (water dissolution)

To this end, a normalized concentration $c' = \frac{c_i}{c_{\text{solid}}}$ is defined, where c_{solid} is the concentration of atoms in the metal and c_i is the concentration of multiple ionic species where i equals, e.g., Mg^{2+} ,Na^+, Cl^- , H^+, OH^- , etc.)

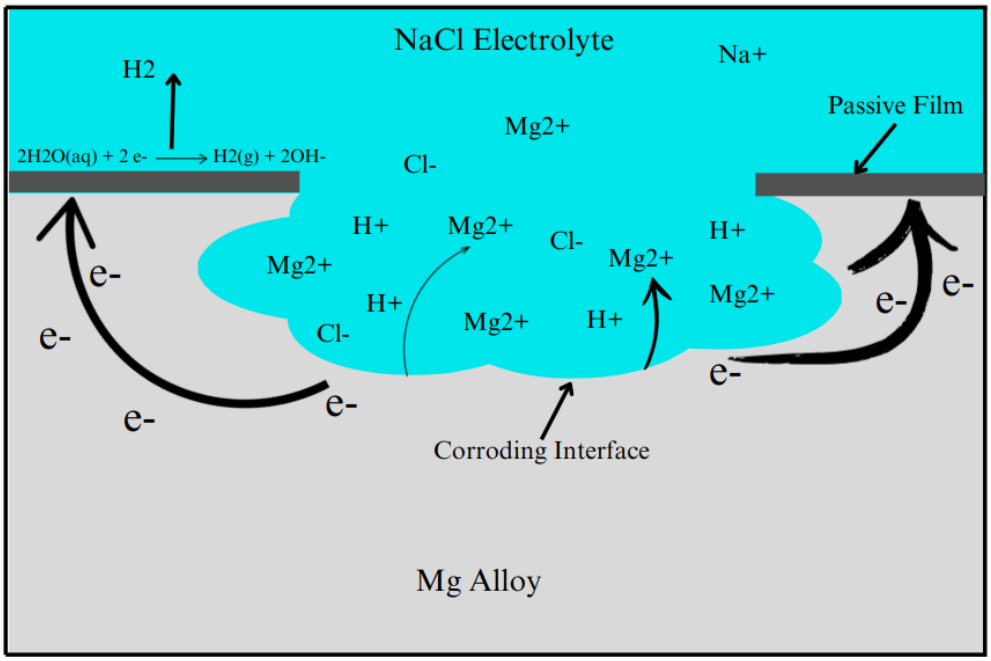

Figure 3.2: conceptual figure for corrosion in Mg alloys.

3.2.2 Phase field governing equations

The decrease of the system F's free energy is the primary driver of every phase transition. This free energy in a phase field model is made up of the interface energy F_{init} and the homogeneous bulk energy F_{bulk}, which are determined by equation 2.2.

$$F = F_{bulk} + F_{init} + F_{elec} = \int [f(c', \phi\ ) + f_{init} + f_{elec}]\, dV \tag{3.1}$$

where $f(c', \phi)$ is the local free energy density, which is a function of c' and ϕ , while f_{init} is the excessive energy associated with the diffuse interface and f_{elec} is the electric energy density.the key difference between various models is the definition of the local free energy density $f(c', \phi)$.The bulk free energy density, $f(c', \phi)$ of the system is adopted from the model proposed by Kim et al (Kim et al., 1999). Each material point in the KKS model is thought to be a combination of two or more phases with comparable chemical potentials but varying concentrations. These presumptions can be stated as follows in the current phase field corrosion model:

$$c' = h(\phi)c'_S + [1 - h(\phi)]c'_L, \tag{3.2}$$

$$\frac{\partial f_S(c'_S)}{\partial c'_S} = \frac{\partial f_L(c'_L)}{\partial c'_L}, \tag{3.3}$$

where the normalized concentrations of the coexisting solid and liquid phases are represented by c'_S and c'_L, respectively, and the free energy densities for each phase are represented by $f_S(c'_S)$ and $f_L(c'_L)$. Furthermore, $h(\phi)$ is a C^∞-continuous interpolation function such that $h(\phi = 0) = 0$ and $h(\phi = 1) = 1$. In this work, we assume $h(\phi) = -2\phi^3 + 3\phi^2$. A similar method can be used to calculate the local free energy density since the concentration at any given location is determined by the weighted sum of the concentrations of solid and liquid substances, i.e.,

$$f(c', \phi) = h(\phi)f_S(c'_S) + [1 - h(\phi)]f_L(c'_L) + wg(\phi), \tag{3.4}$$

where w is the height of the double-well potential $g(\phi) = \phi^2(1-\phi)^2$. It must be noted that in the Cahn–Hilliard equation 3.11, the diffusion of dissolved species is governed by the chemical potential gradient $(\delta f/\delta c')$ instead of the concentration gradient; thus, the proposed model is valid in both dilute and concentrated solutions provided that free

energy density functions used for $f_S(c'_S)$ and $f_L(c'_L)$ are assumed to be parabolic functions, consistent with the literature (Hu et al., 2007). In this paper, we focus mainly on simulating pitting corrosion in dilute solutions, for which the free energy densities can reasonably be approximated as

$$f_S(c'_S) = A(c'_S - c'_{Se})^2, \tag{3.5}$$

$$f_L(c'_L) = A(c'_L - c'_{Le})^2. \tag{3.6}$$

In the above equations, $c'_{Se} = c_{\text{solid}}/c_{\text{solid}} = 1$ and $c'_{Le} = c_{\text{sat}}/c_{\text{solid}}$ are the normalized equilibrium concentrations for the solid and liquid phases, respectively. In addition, A is the curvature of the free energy density, which is assumed to be similar for the solid and liquid phases. Combining equation 3.4, 3.5 and 3.6 returns

$$f(c', \phi) = A[c' - h(\phi)(c'_{Se} - c'_{Le}) - c'_{Le}] + wg(\phi), \tag{3.7}$$

the following expression for the chemical free energy density associated with the metal ion concentrationThe value of A is computed such that the phase transformation driving force in the resulting approximate system is similar to that of the actual thermodynamic system. Using an appropriate local free energy density $f(c', \phi)$, together with the assumptions made in 3.2 and 3.3, one can then simulate the propagation of a corrosion pit by solving the Allen–Cahn and Cahn–Hilliard equations given in (3.10) and (3.11), respectively.

The excessive interface energy arises from the inhomogeneity within the interface region, which can be written as a function of the field variable gradients as (Mai et al., 2016)

$$f_{init} = \frac{\alpha_\phi}{2} (\nabla\phi)^2 + \frac{\alpha_c}{2} (\nabla c')^2 \tag{3.8}$$

In equation 3.8, α_c and α_ϕ are the gradient energy coefficients associated with the concentration and phase fields, respectively.The electric free energy density of the system subjected to a net electric potential in the electrolyte can be written as (Jefimenko, 1989)

$$f_{elec} = F\varphi \quad \sum_i z_i c_i \tag{3.9}$$

where where F is Faraday's constant, φ is electric potential and z_i is the charge number of component i. To assure the reduction of the free energy during the corrosion process, the phase field governing equations are derived by minimizing F via variational differentiation (Abubakar et al., 2015 Boettinger et al., 2002), which yields equations 3.10 and 3.11 represent the general form of a phase field model

$$\frac{\partial \phi(x,t)}{\partial t} = -L\frac{\delta \mathcal{F}}{\delta \phi} = -L\left(\frac{\partial f}{\partial \phi} - \alpha_\phi \nabla^2 \phi\right) \tag{3.10}$$

$$\frac{\partial c'(x,t)}{\partial t} = \nabla \cdot M\nabla\frac{\delta \mathcal{F}}{\delta c'} = \nabla \cdot M\nabla\left(\frac{\partial f}{\partial c'} - \alpha_c \nabla^2 c'\right) \tag{3.11}$$

where L is the interface kinetics parameter and M is the diffusion mobility for mass transport. Eqs. 3.10 and 3.11 are referred to as the AllenCahn and CahnHilliard equations, respectively. Note that, in practice, only one of the gradient terms $\nabla c'$or $\nabla\phi$ would be sufficient to approximate the energy contribution from the diffuse interface; thus the concentration gradient energy coefficient α_c is assumed to be 0 for simplicity.

The distribution of electrostatic potential φ can be estimated by the following Poisson-type equation (Tsuyuki et al., 2018)

$$\nabla \cdot (\kappa \nabla \varphi) = n_M F c_{solid}\frac{\partial \phi}{\partial t} \tag{3.12}$$

where

$$\kappa = h(\phi)\kappa_s + [1 - h(\phi)]\frac{F^2}{R_g T}\left(c_M c_{solid} D_M n_M^2 + \sum_i c_i D_i n_i^2\right) \tag{3.13}$$

κ is the electric conductivity

3.3 Phase Field Parameters

The current phase field corrosion model shows a correlation between the interface energy and its thickness l and the gradient energy coefficient α_ϕ and the height of the double well potential w (Mai et al., 2016). According to literature, the interface energy σ and its thickness l are connected to the gradient energy coefficient α_ϕ and the height of the double well potential w in the current phase field corrosion model (Mai et al., 2016). The equivalent valency of an alloy depends on the oxidation states of its primary elements and their proportions. For AZ31, which consists mainly of magnesium (Mg), aluminum (Al), and zinc (Zn), the typical oxidation states are:

- Mg: +2 (96%)
- Al: +3 (3%)
- Zn: +2 (1%)

The weighted average valency (V_{eq}) is computed as:

$$V_{eq} = (f_{Mg} \times V_{Mg}) + (f_{Al} \times V_{Al}) + (f_{Zn} \times V_{Zn}) \tag{3.14}$$

where:

$$f_{Mg} = 0.96, \quad V_{Mg} = 2$$
$$f_{Al} = 0.03, \quad V_{Al} = 3$$
$$f_{Zn} = 0.01, \quad V_{Zn} = 2$$

Substituting these values:

$$V_{eq} = (0.96 \times 2) + (0.03 \times 3) + (0.01 \times 2) = 1.92 + 0.09 + 0.02 = 2.21 \tag{3.15}$$

Thus, the equivalent valency of AZ31 alloy is approximately **2.2**. Since magnesium is the most reactive and soluble metal, the saturation concentration is determined primarily by Mg dissolution. In pure water, Magnesiumchloride has a solubility of approximately $542g/L$, and the molar density of Magnesium Chloride is $95.21g/mol$. Given that AZ31 contains 96% magnesium, its saturation concentration can be estimated as:

$$C_{sat} = 0.96 \times (542/95.21)\ \text{M} = 5.7\ \text{M} \tag{3.16}$$

The saturation concentration of AZ31 in 1M NaCl solution at STP is approximately **5.7 mol/L** (Mai et al., 2016; Kovacevic et al., 2023).

The diffusion mobility coefficient is denoted by M = D/(2A), where D is the diffusion coefficient and A is a temperature-dependent free energy density proportionality constant, commonly referred to as the free energy density curvature. L is the so-called phase-field mobility parameter. The interface energy per area σ and its thickness ℓ can be connected to the height w and gradient energy coefficient α as follows:

$$\sigma = \sqrt{\frac{\alpha w}{18}} \quad \text{and} \quad \ell = \sqrt{\frac{8\alpha}{w}}.$$

Table 3.1: The PF model parameters used in the simulations.

Parameter	**Value**
Interface energy σ	10 J/m^2
Interface thickness ℓ	1 μ m
Temperature T	293.15 K
Diffusion coefficient D_M	10^{-10} m^2/s
Interface Kinetics Coefficient, L	2 m^3/Js
Average charge number n_M	2.2
Free energy density curvature A	5.35 J/mol
Avg concentration of metal c_{solid}	71.44 mol/L
Avg saturation concentration c_{sat}	5.7 mol/L
Anodic charge transfer coefficient a_a	0.5
Initial electrolyte pH	7.0
Initial NaCl concentration	1 M
Applied potential φ	-0.45 V

Here is a quantifiable relationship between the density of anodic or corrosion current i and the parameter for phase field mobility L. Given the activation-controlled corrosion conditions, Faraday's second rule for electrolysis relates the velocity of the corrosion front v_n to i:

$$v_n = \frac{i}{zFc_{\text{solid}}} \tag{3.17}$$

Here, z is the average ionic charge number ($z = 2.2$ for AZ31) and F is Faraday's constant. Since $v_n \propto \frac{d\phi}{dt}$, this implies that the coefficient of mobility the interface or interface kinetic coefficient which is proportional to the corrosion current density: $L \propto i$. Consequently, if the proportionality value for a different current (e.g., L_b/i_b) is known, the corresponding mobility coefficient (L_a) for any current density of corrosion (e.g., i_a) may be easily found; for instance,

$$L_a = i_a \frac{L_b}{i_b} \tag{3.18}$$

Consequently, it is possible to perform a uniform corrosion simulation with an arbitrary L that is small enough to fall inside the activation controlled mode fo corrosion,

calculated the velocity of corroding interface v_n, and estimated the current level of density associated with that L using Equation 3.17. For any given corrosion current density, the interface mobility coefficient can be found using Equation 3.18 once the L/i ratio is known. Curvature of the free energy density A, concentration of Magnesium in solid phase c_{solid}, equilibrium concentration or concentration of Magnesium ion at saturation c_{sat}, energy density at interface σ, and length scale for order parameter or phase field ℓ are the remaining parameters of the model. The slope of the coefficient of energy α and the elevation of the barrier energy related with the double-well potential w are determined by the choice of the last two.

For the magnessium based model system, the concentration quantities are well-established: $c_{\text{solid}} = 71.44$ mol/L and the saturaturation concentration $c_{\text{sat}} = 0.57$ mol/L was calculated on the basis of mass density of AZ31 alloy and mass density of Magnesium Chloride. For both liquid and solid phases, the Gibbs (chemical) free energy density is often estimated using parabolic functions and the option $A = 5.35 \times 10^7$ N/m^2; however, this option could potentially Lastly, a Butler-Volmer-type equation may be used to determine the phase-field mobility coefficient L by taking advantage of the analogy between it and the corrosion current density i.

$$L = L_0 \left[\exp\left(\frac{\alpha_a z M F \eta}{RT} \right) - \exp\left(\frac{(\alpha_a - 1) z M F \eta}{RT} \right) \right] \tag{3.19}$$

where the anodic charge transfer coefficient is α_a. Thus, through the link between L, η, and φ_1, changes in the electrolyte potential have an impact on the phase field evolution equation. Because of the electromigration term, the electrostatic potential also affects the movement of ionic species. Lastly, the phase-field, which explains how electrons are created, and the concentration of ionic species, which affects the electrolyte conductivity, both have an impact on the electrolyte potential calculation. These couplings draw attention to the intricate processes that underlie corrosion and the necessity of using coupled electro-chemo-mechanical models to represent them.

Convergence issues arise from the different rate of reaction and kinetics of each process from a numerical standpoint. However, stabilization techniques that greatly reduce the ensuing numerical oscillations have been devised, such as aggregated integration systems.

3.4 Model Implementation in MOOSE

To model the corrosion simulation of AZ31 in the MOOSE framework, a computational domain of size 120×120 µm is considered, with the lower 85 µm representing the solid metal, 10 µm thick layer represents the remaining upper representing the electrolyte. The length of the hole is taken 10 µm in the middle where the passive film is initially dissolved. This geometry sets initial conditions as nucleated pit. The interface between metal and electrolyte is explicitly defined to capture the electrochemical interactions and the evolution of corrosion. The alloy surface is exposed to NaCl-based electrolyte solution through the interface. The electrochemical parameters presented in 3.1 used unless otherwise stated.

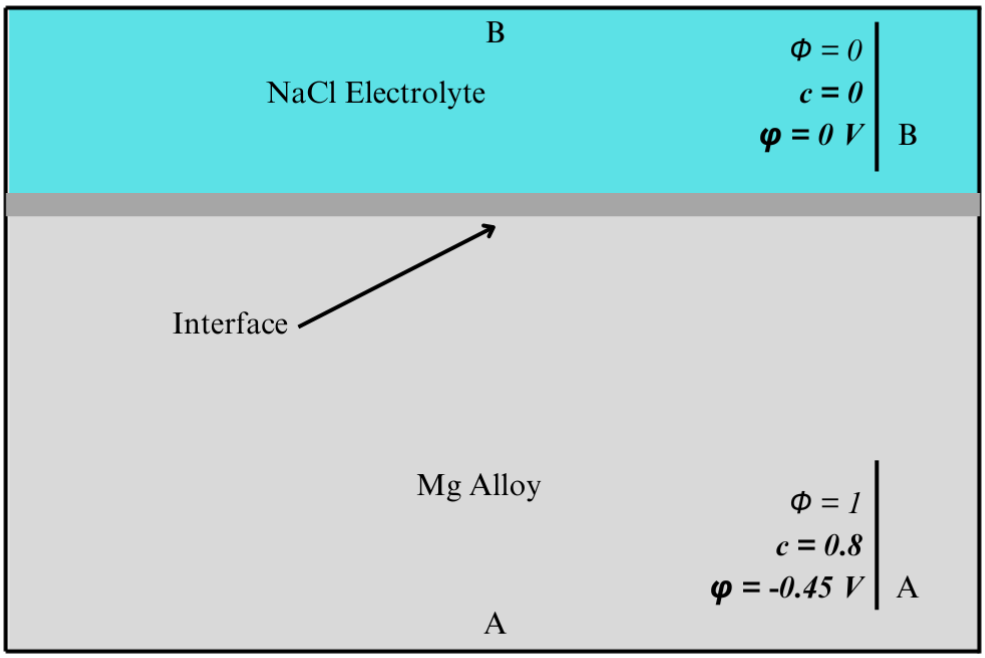

Figure 3.3: Electrochemical corrosion from flat surface: geometric setup, initial and boundary conditions.

Simulation setup:

The simulation setup for studying the electro-chemical corrosion of magnesium alloys was designed using a finite element approach, with a well-structured configuration defined in the input file. The computational domain was created as a two-dimensional space using a generated mesh of quadrilateral elements (QUAD4). The mesh consisted of 30 elements

along both the x and y directions, forming a 30×30 grid. The physical dimensions of the domain were set from 0 to 120 μm along both the x and y axes, while the z-dimension was not considered, reinforcing the two-dimensional nature of the simulation.

The boundary conditions played a crucial role in establishing the electrochemical environment for the corrosion study. Dirichlet boundary conditions were applied to control both the potential and concentration fields. At the bottom boundary, the electrochemical potential ('pot') was fixed at -0.45 V, while the top boundary was assigned a potential value of 0 V. Additionally, the concentration of active species ('ca') on the top boundary was set to 0.7978, representing specific electrochemical characteristics essential for modeling the corrosion behavior. For capturing the time-dependent nature of the corrosion process, a transient solver was employed. The Preconditioned Jacobian-Free Newton-Krylov (PJFNK) (Knoll and Keyes, 2004) method was chosen due to its efficiency and robustness in handling non-linear systems. The solver configuration included a maximum of 50 linear iterations and 20 nonlinear iterations, with tolerances set at 1.0×10^{-4} for the linear solver and 1.0×10^{-10} and 1.0×10^{-11} for the relative and absolute nonlinear solver tolerances, respectively. The simulation was designed to run until an end time of 6.00×10^{30}, ensuring sufficient duration to observe long-term corrosion effects. Time-stepping was managed using an adaptive scheme ('IterationAdaptiveDT'), which adjusted the time step size based on solver performance. The initial time step was set at 0.005, with a cutback factor of 0.8 and a growth factor of 1.1 to maintain stability and efficiency. An optimal iteration count of 10 was targeted to balance accuracy and computational cost. To further enhance the resolution of evolving corrosion interfaces, adaptive mesh refinement (AMR) was implemented. The initial mesh underwent two adaptation cycles to better capture initial conditions. During the simulation, elements with high error were refined with a fraction of 0.9, while elements with low error were coarsened with a fraction of 0.1. The maximum refinement level was capped at 2, ensuring that the mesh retained an optimal balance between resolution and computational efficiency. The error weighting was equally distributed between the parameters 'eta1' and 'eta2', reflecting their combined importance in driving the adaptive strategy. This setup allows for a detailed investigation of AZ31 corrosion behavior under realistic electrochemical conditions, facilitating comparisons with experimental data.

For the simulation of pit surface the geometry of the system was taken as shown in figure 3.4. The size of computational domain is same as in uniform corrosion case 3.3 that is 120×120 µm is considered, with the lower 89.5 µm representing the solid metal and the remaining upper representing the electrolyte. The interface between metal and electrolyte is explicitly defined to capture the electrochemical interactions and the evolution of corrosion. The alloy surface is exposed to NaCl-based electrolyte solution through a small pit on the interface , which has a length of 10 μm and all other regions of alloy is separated by the presence of a passive film since, we presume that the pit has nucleated as a result of the localized rupture of the passive film.

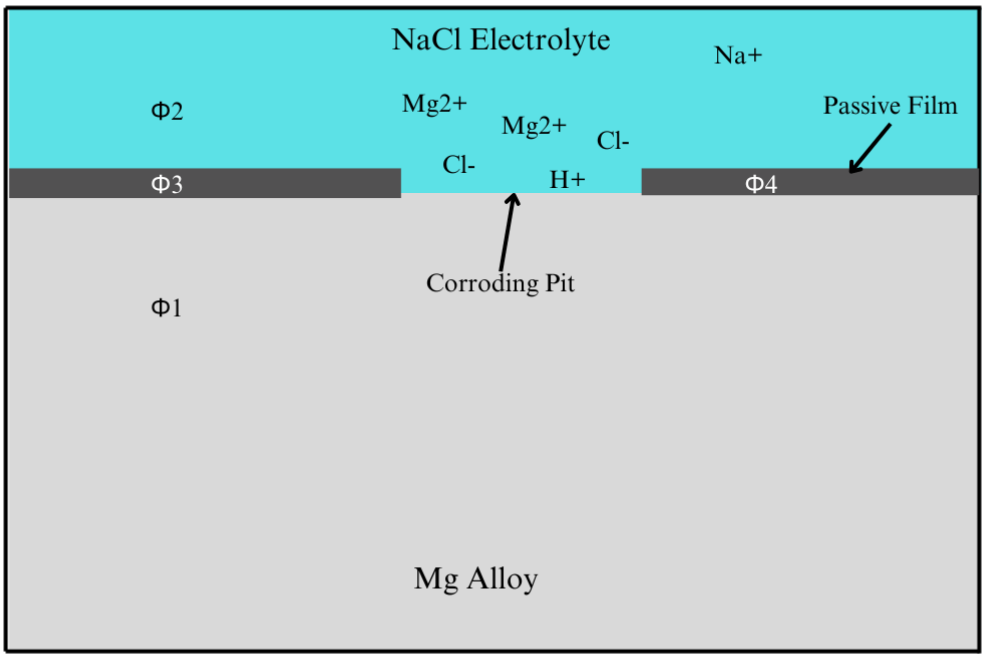

Figure 3.4: Electrochemical corrosion from pit surface and passive film with four order parameter

The same computational domain with generated mesh of quadrilateral elements (QUAD4) was used as in the the cse of uniform corrosion. The mesh consisted of 40 elements along both the x and y directions, forming a 40×40 grid. The physical dimensions of the domain were set from 0 to 120 μm along both the x and y axes, while the z-dimension was not considered, reinforcing the two-dimensional nature of the simulation. Six key phase field

variables were considered for pit simulation anong which four were order parameter (ϕ), one concentration of metal ions (C), and one electric potential distribution (V) were initialized to represent phase evolution, ion diffusion, and electrochemical interactions. Initial conditions and boundary conditions are same as in uniform corrosion except the change in electrostatic potential of electrode. Two cases with different electrostatic potential are considered, one with -0.45V and the other wit -0.3V. The initial and boundary conditions for the order parameters were 1 in the regions as shown in figure 3.4 and elsewhere its value is zero with smooth transition at boundaries. Material properties, including diffusion coefficients and reaction kinetics, are same as before with little revision in interface kinetic coefficient. The kinetic interface parameter was re-calibrated with experimental data from the literature and its value is taken as 10 m^3/Js. The properties of passive layer set by scaling the properties of metal electrode such that degradation in passive layer is negligible. The numerical solver employs implicit or explicit time integration with adaptive time-stepping to ensure stability and accuracy, while convergence criteria dictate the precision of the iterative solution.

This simulation setup is very similar to the 1D pencil electrode setup and also renders uniform corrosion but still the geometery choosen 2D for proper visualization of results as well as the set can be used for pitting simulation. The corrosion simulation of AZ31 Magnesium alloy in 1M NaCl solution using the MOOSE framework reveals significant insights into its electrochemical behavior. The phase field (PF) model utilized to simulate the evolution of corrosion in a two-dimensional framework successfully captures the effects of interface evolution, metal dissolution, and electric potential variation. Simulations were conducted at a temperature of 293.15 K (20 °C) with a metal potential set at -0.45 V (over potential) relative to the standard hydrogen electrode (SHE) in a 1 M NaCl solution in the bulk electrolyte side. The results of the PF simulations, particularly in terms of the depth of corrosion, were compared with the experimental data obtained from the literature. The simulations lasted for 0.8 seconds as in the time frame of 0.8 seconds as all the metal surfaces corroded into metal ions. The reduction in the area of electrode surface is plotted as a function of time shown in Figure 4.1 which can also be interpreted as the rate of corrosion or the speed at which the metal electrolyte interface is evolving. Additionally, analysis of the variability of magnesium ion concentration within the electrolyte is also conducted, aligning with methodologies employed in classical numerical models. Also the change in electric potential distribution over the domain is captured.

To visualize the result of the simulation, ParaView 5.7.0 software is utilized. The software reads the output file from MOOSE in exodus format. A glimpse of result visualization in ParaView is shown in figure 4.2.

Corrosion Morphology: The simulation results indicate that AZ31 undergoes corrosion as shown in 4.3, in terms of the phase field contours, which illustrate the evolution of the corrosion front. The phase-field variable shows a progressive dissolution pattern, confirming experimental observations of corrosion process. The results show that dissolution is symmetric over the surface, with corrosion rates being same along the depth direction at all location of the interface due to the symmetricity of the problem. Moreover, results reveal that corrosion rates shows linear behaviour as reported in the results obtained for the pencil electrode test for small corrosion time in literature. If the simulation run time

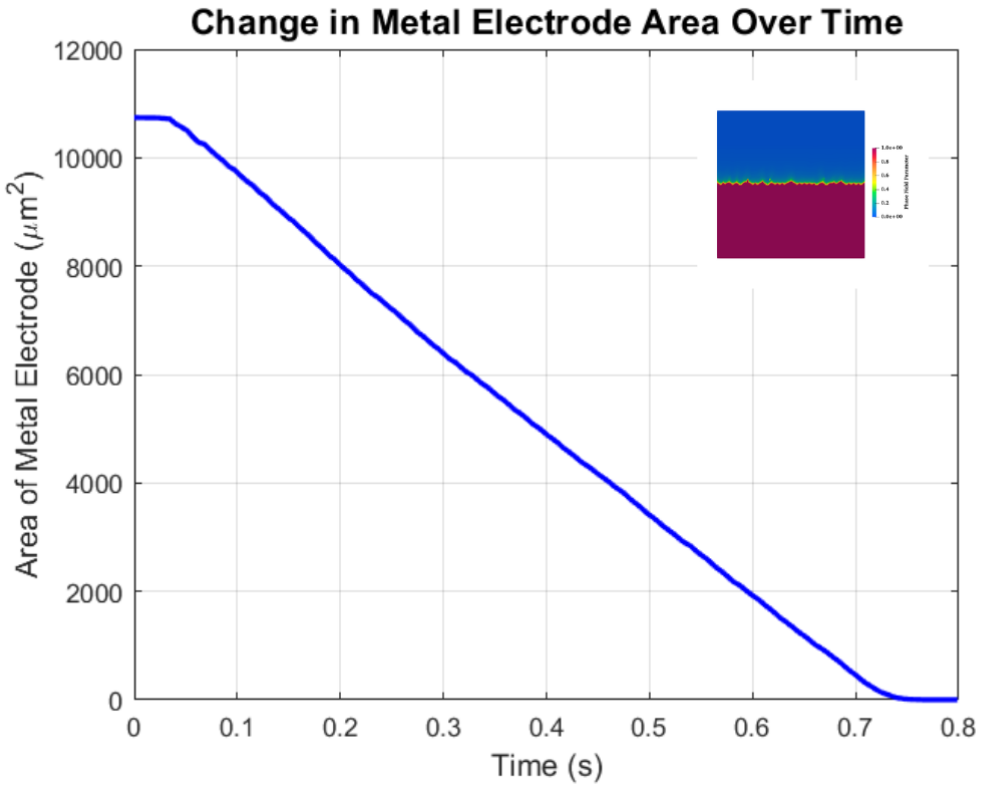

Figure 4.1: Change of Area of Mg electrode with respect to corrosion time

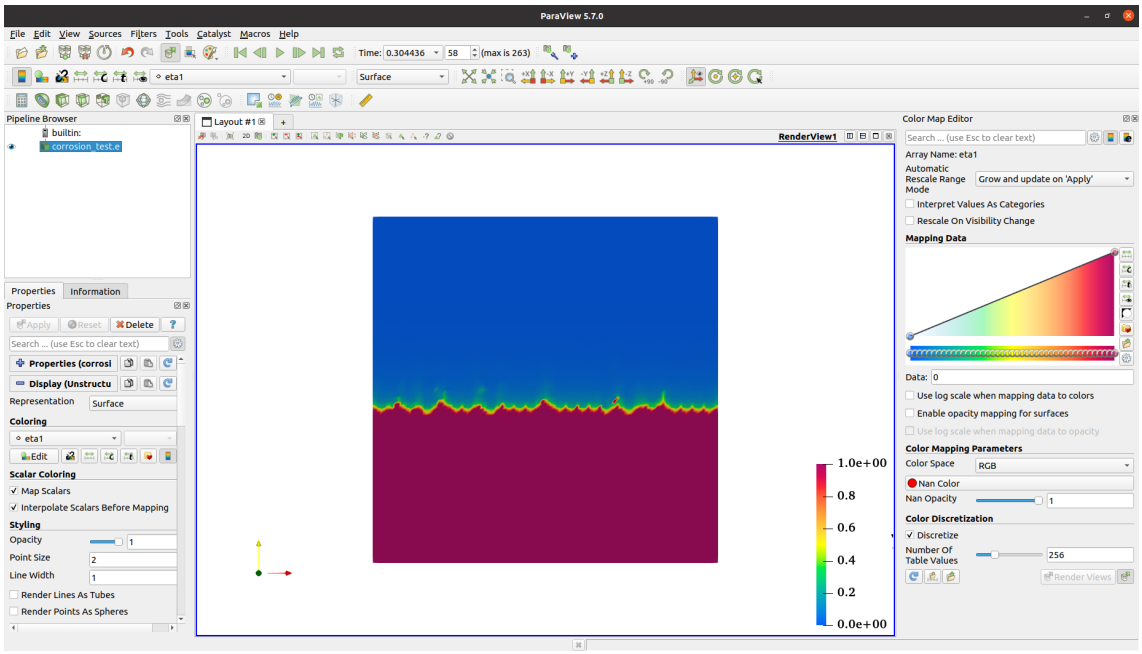

Figure 4.2: Result visualization in ParaView 5.7.0

is increased then the corrosion rate could appear to be non linear (Cui et al., 2023).

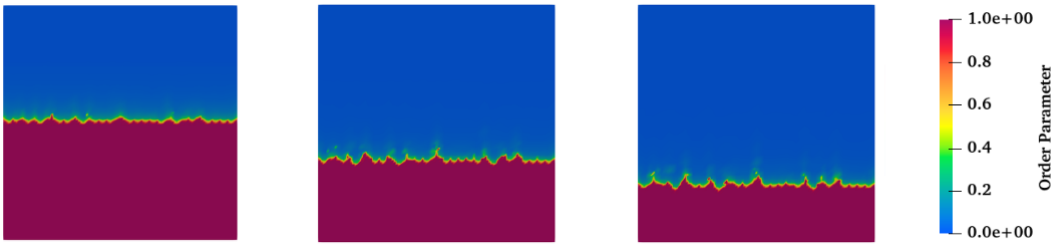

Figure 4.3: phase field contours illustrating the interface evolution over time at 0.2s , 0.4s and 0.5s respetively

Metal Ion Distribution: The non dimensionalized metal ion concentration profiles indicate a gradual increase in Mg^{2+} concentration in the electrolyte. This aligns with the expected saturation concentration range of 0.8, validating the accuracy of the model. It is clear that when the solid metal is dissolved, then the concentration of dissolved metal ions near the interface should increase, and the same appears in the simulation result.

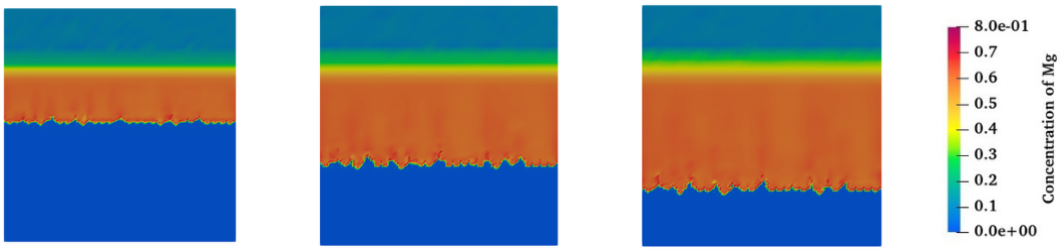

Figure 4.4: Contours of Mg^{2+} ions at times 0.2s , 0.4s and 0.5s respectively

Electrochemical Potential Variation: The electrostatic potential distribution suggests a strong correlation between the anodic and cathodic regions, with the corrosion front advancing as the electrochemical reactions progress. The applied potential influences the dissolution rate, emphasizing the role of external electrical conditions. Analyzing the contours of the electric potential, it seems to be steady over time with only a slight change. It might be due to the reason that as over-potential increases, $[H^+]$ ion concentration also rises, corresponding to the enhanced rates of hydrolysis of metal ions. This increase in positive charge is balanced by the migration of chloride ions towards the metal-electrolyte interface.

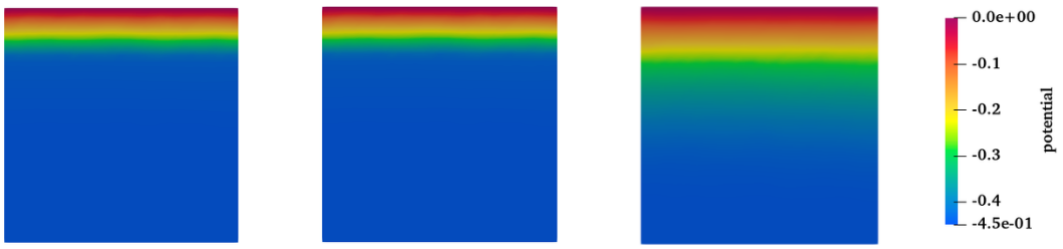

Figure 4.5: Contours of electrostatic potential at times different times 0.2s , 0.4s and 0.5s respetively

At this point, the results of the simulations can be qualitatively validated by comparing them with the results of similar simulation (Ansari et al., 2018; Cui et al., 2023, 2022). It is found that the model developed in this paper seems a promising approach for simulating complex corrosion phenomena of Magnesium alloy, but still a lot of modifications are required to make the model allign with quantative results of past experiments.

4.1 Behaviour with 0.45V Overpotential

At an applied overpotential of 0.45V, the simulation exhibits an aggressive and highly localized corrosion behavior. The contours of the order parameter ϕ clearly show a rapid transition from the metallic phase ($\phi = 1$) to the electrolyte phase ($\phi = 0$), indicating a fast-moving corrosion front. This rapid degradation reflects the high electrochemical driving force associated with the elevated overpotential, which significantly accelerates the anodic dissolution of the magnesium alloy.

Figure 4.6: Phase field contours for pit at 0.45V overpotential illustrating the interface evolution over time

The magnesium ion concentration c in the electrolyte increases sharply in the localized corroded regions, particularly inside the developing pit. This accumulation of Mg^{2+} ions is a direct consequence of the intense anodic reaction occurring at the interface. Over

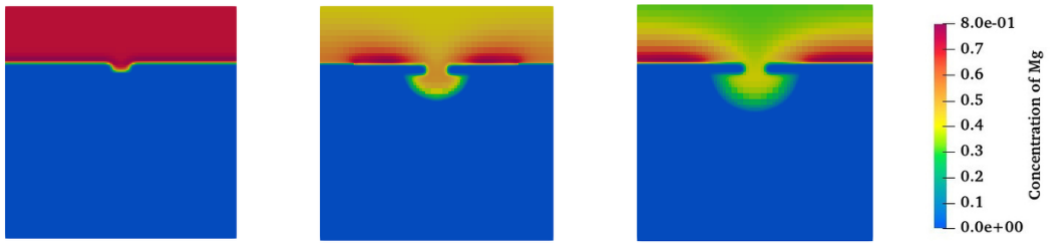

Figure 4.7: Contours of Mg^{2+} ions for pit at 0.45V overpotential

time, the pit deepens and becomes more focused, while the surrounding areas of the metal remain relatively unaffected. This behavior is consistent with experimental observations of pitting corrosion in magnesium alloys under aggressive electrochemical conditions.

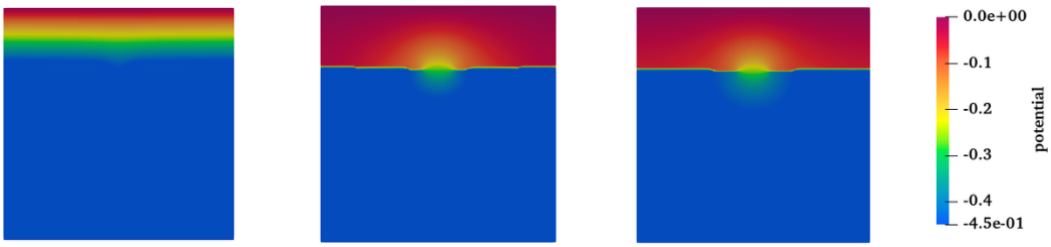

Figure 4.8: Contours of electrostatic potential for pit at 0.45V overpotential

The electric potential distribution φ reveals steep gradients concentrated near the interface between the metal and the electrolyte. These gradients suggest strong localization of the electric field, which contributes to the initiation and propagation of pit like features. The current density, governed by the Butler–Volmer kinetics, is also highly localized, further driving the corrosion in specific regions.

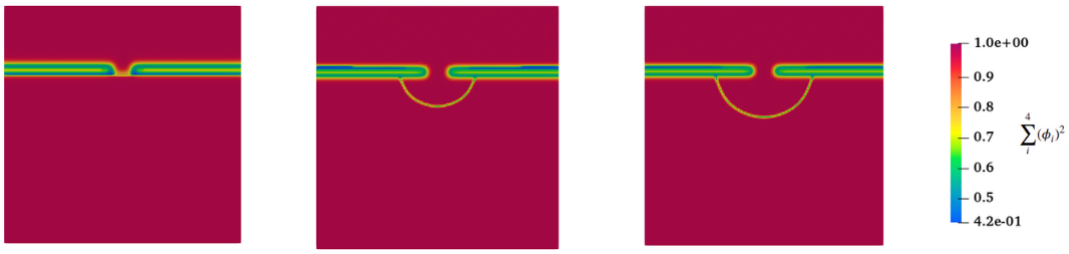

Figure 4.9: Phase evolution for 4 phases over the domain for 0.45V. Scale bar magnitudes are denoted as 1.0 within phases and are less than 1 at phase boundaries

Overall, the high overpotential induces a non-uniform dissolution morphology characterized by the formation of deep pits and sharp interfaces. The simulation results confirm

that increased electrochemical driving forces promote instability at the corrosion front, leading to the development of localized corrosion features.

4.2 Behaviour with 0.3V Overpotential

When the applied overpotential is reduced to 0.3V, the simulated corrosion behavior changes significantly. The order parameter ϕ evolves more gradually, and the transition from metal to electrolyte occurs more uniformly and widely. This indicates that the corrosion front is advancing slowly and evenly across the exposed surface, which is characteristic of generalized corrosion.

Figure 4.10: Phase field contours for pit at 0.3V overpotential illustrating the interface evolution over time

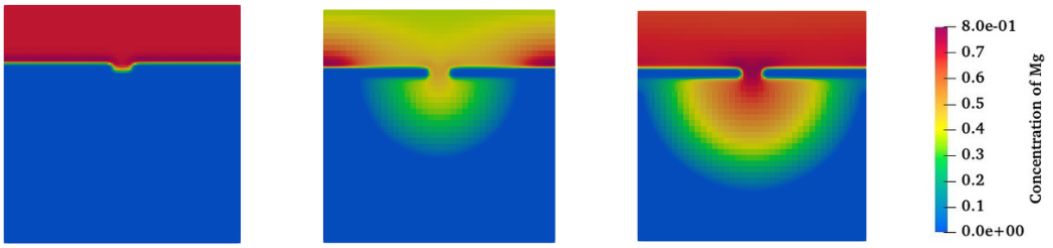

Figure 4.11: Contours of Mg^{2+} ions for pit at 0.3V overpotential

The magnesium ion concentration c increases at a slower rate compared to the 0.45V case. The distribution of Mg^{2+} ions remains relatively uniform in the electrolyte, indicating a broader and more homogeneous release of ions. This supports the conclusion that corrosion is proceeding in a more controlled and distributed fashion.

The electric potential η shows a smoother and less steep distribution across the domain. The electric field is less localized, resulting in a lower and more distributed current density.

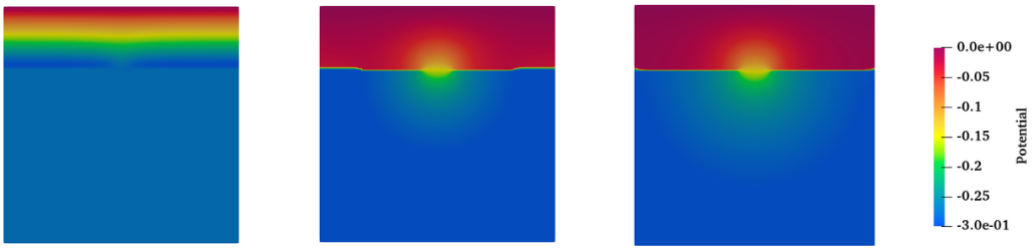

Figure 4.12: Contours of electrostatic potential for pit at 0.3V overpotential

This decrease in electrochemical activity slows the dissolution rate and minimizes the occurrence of localized attack.

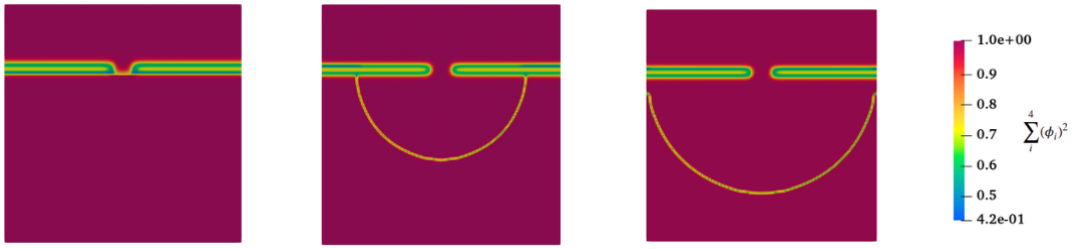

Figure 4.13: Phase evolution for 4 phases over the domain for 0.3V. Scale bar magnitudes are denoted as 1.0 within phases and are less than 1 at phase boundaries

The resulting corrosion morphology is relatively flat and smooth, without the formation of deep pits. The overall depth of corrosion is also shallower, and the simulation demonstrates the stabilizing effect of the lower overpotential on the corrosion front. These findings are in good agreement with the theory that lower overpotentials reduce the kinetic rate of anodic dissolution and lead to more uniform degradation of the metal.

4.3 Comparison

A direct comparison between the two overpotential conditions illustrates the critical role of applied electrochemical potential in determining the corrosion morphology.

- At **0.45V**, the system experiences a high corrosion rate with localized damage, leading to the formation of pits. The electric potential and the cation concentration exhibit sharp spatial variations that reinforce the instability of the corrosion front.
- At **0.3V**, the corrosion process is more stable and generalized. The electric field and ion flux are less concentrated, resulting in a more uniform material loss across

the surface.

- The comparative analysis of the corrosion rate as in figure 4.14 showed that the corrosion rate in the case of a higher overpotential was higher, aligning with the theoretical predictions.

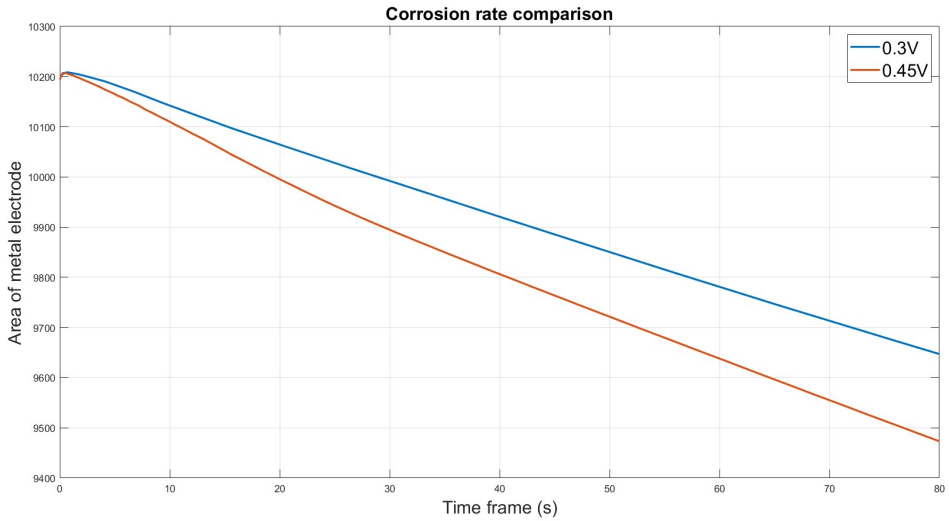

Figure 4.14: Comparison of corrosion rate for 0.45V and 0.3V overpotential

These results validate the ability of the phase field model to capture distinct corrosion behaviors under different electrochemical conditions. The coupling of the order parameter, the electric potential, and the concentration of ions provides a powerful framework for simulated uniform and localized corrosion processes. The model effectively reflects how electrochemical driving forces influence the morphology and kinetics of corrosion in magnesium alloys.

CHAPTER FIVE: CONCLUSIONS AND RECOMMENDATIONS

5.1 Conclusions

Based on the task performed on the basis of specific objectives, the following conclusions were inferred.

- A comprehensive literature review provided essential material properties, initial conditions, and boundary conditions for AZ31 Mg alloy. The equivalent valency, diffusion coefficients, interfacial energy, and electrochemical parameters were identified to ensure accurate simulation setup. These parameters were crucial in defining the corrosion behavior under NaCl electrolyte conditions.

- The phase field method successfully solved the corrosion evolution by incorporating key variables: order parameter, metal ion concentration, and electric potential distribution. The numerical model effectively captured the dissolution kinetics, ion migration, and electrochemical interactions, validating the phase field approach as a viable method for corrosion modeling.

- The simulation results demonstrated a progressive dissolution pattern, with corrosion rates showing initial linear behavior. The metal ion distribution and electrochemical potential contours aligned well with experimental trends, confirming the accuracy of the model. The results also indicated that longer simulation times could reveal non-linear corrosion behavior, requiring further investigation. The corrosion rate obtained in case of uniform corrosion was 0.1 mm/s. In case of pitting corrosion with revised mobility coefficients the corrosion rate was obtained as 6.3 mm/day for 0.45V overpotential and 4.8 mm/day. The results for pitting corrosion was much closer to the experimental value in comparison to uniform corrosion.

5.2 Recommendations

Future studies should include experimental validation of these material properties to refine and improve numerical modeling accuracy. Additionally, considering environmental effects such as temperature fluctuations and varying electrolyte compositions can enhance model reliability.

Further refinement of the numerical solver, including adaptive meshing techniques and higher computational efficiency, is recommended. Extending the model to three-dimensional simulations can provide a more comprehensive understanding of localized corrosion effects. Validation against experimental corrosion tests should be prioritized to assess the model's predictive capability. The mobility coefficients still needs more rectification at the same time the numercal covergence needs to be maintained. The tuninig of input parameters and the numerical solvers is requred in further study. Additionally, incorporating real-time monitoring techniques in experimental setups can provide more accurate benchmarking data for future improvements in corrosion modeling.

REFERENCES

Kainer, K. U. (2003). *Magnesium alloys and technology*. John Wiley & Sons.

Xu, T., Yang, Y., Peng, X., Song, J., & Pan, F. (2019). Overview of advancement and development trend on magnesium alloy. *Journal of Magnesium and Alloys*, *7*(3), 536–544.

Hou, L., Li, Z., Pan, Y., Du, L., Li, X., Zheng, Y., & Li, L. (2014). In vitro and in vivo studies on biodegradable magnesium alloy. *Progress in Natural Science: Materials International*, *24*(5), 466–471.

Avedesian, M. M. (1999). Asm specialty handbook-magnesium and magnesium alloys.

Song, J., She, J., Chen, D., & Pan, F. (2020). Latest research advances on magnesium and magnesium alloys worldwide. *Journal of Magnesium and Alloys*, *8*(1), 1–41.

Gusieva, K., Davies, C., Scully, J., & Birbilis, N. (2015). Corrosion of magnesium alloys: The role of alloying. *International Materials Reviews*, *60*(3), 169–194.

Jafarzadeh, S., Chen, Z., & Bobaru, F. (2019). Computational modeling of pitting corrosion. *Corrosion reviews*, *37*(5), 419–439.

Taheri, M., Phillips, R., Kish, J., & Botton, G. (2012). Analysis of the surface film formed on mg by exposure to water using a fib cross-section and stem–eds. *Corrosion Science*, *59*, 222–228.

McCafferty, E., & McCafferty, E. (2010). Thermodynamics of corrosion: Pourbaix diagrams. *Introduction to corrosion science*, 95–117.

Makar, G., & Kruger, J. (1993). Corrosion of magnesium. *International materials reviews*, *38*(3), 138–153.

Revie, R. W. (2008). *Corrosion and corrosion control: An introduction to corrosion science and engineering*. John Wiley & Sons.

Martin, H. J., Horstemeyer, M., & Wang, P. T. (2011). Structure–property quantification of corrosion pitting under immersion and salt-spray environments on an extruded az61 magnesium alloy. *Corrosion Science*, *53*(4), 1348–1361.

Ernst, P., & Newman, R. (2002). Pit growth studies in stainless steel foils. i. introduction and pit growth kinetics. *Corrosion Science*, *44*(5), 927–941.

Sharland, S. (1987). A review of the theoretical modelling of crevice and pitting corrosion. *Corrosion science*, *27*(3), 289–323.

Walton, J. C. (1990). Mathematical modeling of mass transport and chemical reaction in crevice and pitting corrosion. *Corrosion Science*, *30*(8-9), 915–928.

Tait, W. S. (2018). Electrochemical corrosion basics, 97–115.

Buchanan, R., & Stansbury, E. (2005). Electrochemical corrosion. In *Handbook of environmental degradation of materials* (pp. 81–103). Elsevier.

Keithley Instruments, I. (1984). *Low level measurements: For effective low current, low voltage, and high impedance measurements*. Keithley Instruments.

Vetter, K. J. (2013). *Electrochemical kinetics: Theoretical aspects*. Elsevier.

Frankel, G. (2016). Fundamentals of corrosion kinetics. *Active protective coatings: new-generation coatings for metals*, 17–32.

Yu, X., Wan, F., & Guo, Y. (2016). Micromechanics modeling of skin panel with pitting corrosion for aircraft structural health monitoring. *2016 IEEE International Conference on Prognostics and Health Management (ICPHM)*, 1–8.

Akpanyung, K., & Loto, R. (2019). Pitting corrosion evaluation: A review. *Journal of Physics: Conference Series*, *1378*(2), 022088.

Esmaily, M., Svensson, J., Fajardo, S., Birbilis, N., Frankel, G. S., Virtanen, S., Arrabal, R., Thomas, S., & Johansson, L. (2017). Fundamentals and advances in magnesium alloy corrosion. *Progress in Materials Science*, *89*, 92–193.

Frankel, G. (1998). Pitting corrosion of metals: A review of the critical factors. *Journal of the Electrochemical society*, *145*(6), 2186.

Jones, D. A. (1996). Principles and prevention. *Corrosion*, *2*, 168.

Marcus, P., & Oudar, J. (2002). *Corrosion mechanisms in theory and practice*. Marcel Dekker New York.

Pourbaix, M. (1966). Atlas of electrochemical equilibria in aqueous solutions. *NACE*.

Taheri, M., & Kish, J. (2012). Nature of surface film formed on mg exposed to 1 m naoh. *Journal of The Electrochemical Society*, *160*(1), C36.

Li, S., Bacco, A. C., Birbilis, N., & Cong, H. (2016). Passivation and potential fluctuation of mg alloy az31b in alkaline environments. *Corrosion Science*, *112*, 596–610.

Sarkar, S., Warner, J. E., & Aquino, W. (2012). A numerical framework for the modeling of corrosive dissolution. *Corrosion science*, *65*, 502–511.

Xiao, J., & Chaudhuri, S. (2011). Predictive modeling of localized corrosion: An application to aluminum alloys. *Electrochimica Acta*, *56*(16), 5630–5641.

Li, Y., Hu, S., Sun, X., & Stan, M. (2017). A review: Applications of the phase field method in predicting microstructure and property evolution of irradiated nuclear materials. *npj Computational Materials*, *3*(1), 16.

Mai, W., Soghrati, S., & Buchheit, R. G. (2016). A phase field model for simulating the pitting corrosion. *Corrosion Science*, *110*, 157–166.

Ansari, T. Q., Xiao, Z., Hu, S., Li, Y., Luo, J.-L., & Shi, S.-Q. (2018). Phase-field model of pitting corrosion kinetics in metallic materials. *npj Computational Materials*, *4*(1), 38.

Abubakar, A. A., Akhtar, S. S., & Arif, A. F. M. (2015). Phase field modeling of v2o5 hot corrosion kinetics in thermal barrier coatings. *Computational Materials Science*, *99*, 105–116.

Tsuyuki, C., Yamanaka, A., & Ogimoto, Y. (2018). Phase-field modeling for ph-dependent general and pitting corrosion of iron. *Scientific reports*, *8*(1), 12777.

Cui, C., Ma, R., & Martínez-Pañeda, E. (2023). Electro-chemo-mechanical phase field modeling of localized corrosion: Theory and comsol implementation. *Engineering with Computers*, *39*(6), 3877–3894.

Kovacevic, S., Ali, W., Martínez-Pañeda, E., & LLorca, J. (2023). Phase-field modeling of pitting and mechanically-assisted corrosion of mg alloys for biomedical applications. *Acta Biomaterialia*, *164*, 641–658.

Kim, S. G., Kim, W. T., & Suzuki, T. (1999). Phase-field model for binary alloys. *Physical review e*, *60*(6), 7186.

Hu, S., Murray, J., Weiland, H., Liu, Z., & Chen, L. (2007). Thermodynamic description and growth kinetics of stoichiometric precipitates in the phase-field approach. *Calphad*, *31*(2), 303–312.

Jefimenko, O. D. (1989). Electricity and magnetism: An introduction to the theory of electric and magnetic fields. *(No Title)*.

Boettinger, W. J., Warren, J. A., Beckermann, C., & Karma, A. (2002). Phase-field simulation of solidification. *Annual review of materials research*, *32*(1), 163–194.

Knoll, D. A., & Keyes, D. E. (2004). Jacobian-free newton–krylov methods: A survey of approaches and applications. *Journal of Computational Physics*, *193*(2), 357–397.

Cui, C., Ma, R., & Martínez-Pañeda, E. (2022). A generalised, multi-phase-field theory for dissolution-driven stress corrosion cracking and hydrogen embrittlement. *Journal of the Mechanics and Physics of Solids*, *166*, 104951.

APPENDIX

Pulchowk Campus
Institute of Engineering
Tribhuvan University

SAROJ SHAH <079msmde019.saroj@pcampus.edu.np>

[IOEGC16] Editor Decision
2 messages

Kobid <conference-noreply@ioe.edu.np> Sat, Mar 29, 2025 at 8:13 AM
To: Saroj Kumar Shah <079msmde019.saroj@pcampus.edu.np>

Saroj Kumar Shah:

We are pleased to inform you that your manuscript titled "Modeling Electrochemical Corrosion in Magnesium Alloys Using MOOSE Based Non-linear Phase Field Methods" submitted to 16th IOE Graduate Conference is **Accepted** for presentation in the Conference as well as inclusion in the Peer-Reviewed Proceedings. Please note that inclusion in hard copy proceedings is contingent upon your timely response to further edits, if any, during the publication process.

Reviewer's Comments:

With Warm Regards,
IOEGC-16 Editorial Team

Kobid <conference-noreply@ioe.edu.np> Sat, Mar 29, 2025 at 8:13 AM
To: Saroj Kumar Shah <079msmde019.saroj@pcampus.edu.np>

[Quoted text hidden]

Saroj Kumar Shah

plag_check_saroj_2.pdf

Tribhuvan University

Document Details

Submission ID
trnoid::3117:449364564

Submission Date
Apr 15, 2025, 7:35 PM GMT+5:45

Download Date
Apr 15, 2025, 7:37 PM GMT+5:45

File Name
plag_check_saroj_2.pdf

File Size
2.0 MB

43 Pages

10,613 Words

58,638 Characters

✓iThenticate Page 1 of 49 - Cover Page Submission ID trnoid::3117:449364564

13% Overall Similarity

The combined total of all matches, including overlapping sources, for each database.

Filtered from the Report

- Bibliography
- Quoted Text
- Cited Text
- Small Matches (less than 8 words)

Match Groups

109 Not Cited or Quoted 13%
Matches with neither in-text citation nor quotation marks

0 Missing Quotations 0%
Matches that are still very similar to source material

0 Missing Citation 0%
Matches that have quotation marks, but no in-text citation

0 Cited and Quoted 0%
Matches with in-text citation present, but no quotation marks

Top Sources

9% Internet sources
12% Publications
0% Submitted works (Student Papers)

Integrity Flags

0 Integrity Flags for Review

No suspicious text manipulations found.

Our system's algorithms look deeply at a document for any inconsistencies that would set it apart from a normal submission. If we notice something strange, we flag it for you to review.

A Flag is not necessarily an indicator of a problem. However, we'd recommend you focus your attention there for further review.

Match Groups

- 109 Not Cited or Quoted 13%
  Matches with neither in-text citation nor quotation marks
- 0 Missing Quotations 0%
  Matches that are still very similar to source material
- 0 Missing Citation 0%
  Matches that have quotation marks, but no in-text citation
- 0 Cited and Quoted 0%
  Matches with in-text citation present, but no quotation marks

Top Sources

9% Internet sources
12% Publications
0% Submitted works (Student Papers)

Top Sources

The sources with the highest number of matches within the submission. Overlapping sources will not be displayed.

1	Internet	
flore.unifi.it		1%
2	Internet	
arxiv.org		1%
3	Publication	
Chuanjie Cui, Rujin Ma, Emilio Martínez-Pañeda. "Electro-chemo-mechanical phas...		1%
4	Internet	
zero.sci-hub.se		<1%
5	Internet	
www.nature.com		<1%
6	Internet	
www.researchgate.net		<1%
7	Publication	
Jafarzadeh, Siavash. "Novel and Fast Peridynamic Models for Material Degradatio...		<1%
8	Publication	
Weijie Mai, Soheil Soghrati, Rudolph G. Buchheit. "A phase field model for simulat...		<1%
9	Internet	
acml.engineering.osu.edu		<1%
10	Publication	
Hailong Zhi, Peng Dong, Kewei Li, Linshan Gao, Wenjie Zhou, Hongxia Zhang. "Ph...		<1%

iThenticate Page 3 of 49 - Integrity Overview Submission ID trn:oid:::3117:449364564